Constraining the applicability of organic paleotemperature proxies for the last 90 Myrs

Marijke W. de Bar [a,*], Sebastiaan W. Rampen [a,1], Ellen C. Hopmans [a], Jaap S. Sinninghe Damsté [a,b], Stefan Schouten [a,b,*]

[a] NIOZ Royal Netherlands Institute for Sea Research, and Utrecht University, Department of Microbiology & Biogeochemistry, P.O. Box 59, 1790 AB Den Burg, Texel, the Netherlands
[b] Utrecht University, Faculty of Geosciences, Department of Earth Sciences, P.O. Box 80115, 3508 TC Utrecht, the Netherlands

ABSTRACT

We evaluated changes in the distributions of long-chain alkenones, long-chain diols and GDGTs, lipids commonly used for paleothermometry, over the last 90 Myrs for sediments deposited on the New Jersey shelf (the Bass River site) and assessed potential effects of different ancestral producers and diagenesis on their distributions and their impact on the associated temperature proxies. As reported before, the Paleogene distributions of alkenones are generally similar to those in modern haptophytes, but unusual alkenone distributions, characterized by a dominant di-unsaturated C_{40} alkenone, are observed for Late Cretaceous sediments, suggesting different ancestral source organisms for alkenones in this interval. The isoprenoid GDGT distributions remained comparable to modern-day distributions, suggesting that TEX_{86} can be applied up to ca. 90 Ma. The Miocene long-chain diol distributions are similar to modern-day distributions, but the older sediments reveal unusual distributions, dominated by the C_{28} 1,12- and C_{26} 1,13-diols, suggesting different source organisms before ∼30 Ma. Accordingly, the LDI does not match other paleotemperature proxies, suggesting its applicability might be compromised for sediments older than the Miocene. Our results indicate that of the three proxies, the TEX_{86} seems to be the most applicable for deep time temperature reconstructions.

1. Introduction

Lipid biomarkers have become popular tools in paleoclimate and paleoceanographic studies. Several proxies have been proposed for the reconstruction of past seawater temperature and salinity, terrestrial organic matter input into the marine realm, and continental vegetation changes (see Brocks and Pearson, 2005; Schouten et al., 2013; Luo et al., 2018 for reviews). The most important reconstructed climate parameter is probably sea surface temperature (SST), for which different lipid proxies have been developed. First, the $U_{37}^{K'}$ index (Brassell et al., 1986; Prahl and Wakeham, 1987) based on the unsaturation of long-chain alkenones (LCAs; see Supplementary Fig. S1 for lipid structures), which in modern systems are mainly produced in the open ocean by the haptophytes *Emiliania huxleyi* and *Gephyrocapsa oceanica* (Conte et al., 1995; Volkman et al., 1995).

LCAs observed in marine sediments are typically composed of C_{37}–C_{39} alkyl chains, with two, three or four unsaturations and a keto group at the C-2 (methyl ketone) or C-3 (ethyl ketone) position. The first alkenone unsaturation index was established by Brassell et al. (1986), which included the relative abundance of the di-, tri- and tetra-unsaturated C_{37} LCAs (U_{37}^{K}), followed by the $U_{37}^{K'}$ index proposed by Prahl and Wakeham (1987), which excluded the tetra-unsaturated C_{37} LCA since this LCA did not correlate well with temperature. $U_{37}^{K'}$ values in surface sediments exhibit a strong relationship with SST (Müller et al., 1998; Conte et al., 2006). LCAs are relatively simple to analyze and are often abundant in marine sediments, and hence, the proxy has been regularly applied in paleoclimate reconstructions over the last decades. Evidently, there are also certain issues associated with the $U_{37}^{K'}$ proxy, such as the effect of lateral transport (Ohkouchi et al., 2002; Mollenhauer et al., 2008; Kim et al., 2009), post-depositional oxic degradation (Hoefs et al., 1998) and its upper temperature limit of 29 °C (Prahl and Wakeham, 1987).

The second temperature proxy is TEX_{86} (Schouten et al., 2002, 2013) which is based on the ratio of isoprenoidal glycerol dialkyl glycerol tetraethers (iGDGTs) containing different numbers of cyclopentane moieties (see Supplementary Fig. S1 for lipid structures). These compounds are membrane lipids produced by a range of archaea (Koga and Morii, 2007, Schouten et al., 2013). In the marine environment the main producers of isoprenoidal GDGTs are thought to be Thaumarchaeota (Schouten et al., 2013), and a strong correlation between this index and annual mean SST has been observed for marine surface sediments from all over the world (Schouten et al., 2002; Kim et al., 2008, 2010; Ho et al., 2014; Tierney and Tingley, 2014). Due to the preservation of iGDGT core lipids up to at least the Jurassic, the TEX_{86} proxy has been widely used over these timescales (e.g., Schouten et al., 2004; Forster et al., 2007a, 2007b; Bijl et al., 2009; Littler et al., 2011; Linnert et al., 2014) and its utility has been demonstrated for sediments where other proxies were compromised by diagenesis or associated lipid biomarkers were absent (e.g., Bijl et al., 2009; Liu et al., 2009; Hollis et al., 2012; Schouten et al., 2013 and References cited therein). Also, whereas the upper limit of the $U_{37}^{K'}$ is around 29 °C, the TEX_{86} paleothermometer can record higher temperature as it has not reached unity yet at modern day tropical temperatures, although extrapolation above 30 °C is relatively uncertain and should therefore be done with caution (e.g., Schouten et al., 2003; Tierney and Tingley, 2014 and References cited therein).

However, iGDGTs used in TEX_{86} may not solely derive from the surface mixed layer, but also from deeper living archaea, affecting the TEX_{86} signal, evidenced for both core GDGTs (e.g., Huguet et al., 2007; Lee et al., 2008; Kim et al., 2010, 2012, 2016; Lopes dos Santos et al., 2010; Schouten et al., 2013; Taylor et al., 2013; Chen et al., 2014), as well as for intact polar lipids (IPLs; e.g., Basse et al., 2014; Zhu et al., 2016; Hurley et al., 2018). Additionally, there are several non-thermal biological factors which can potentially affect the TEX_{86}. For instance, it has been shown that the lipid composition of Thaumarchaeota can markedly differ with growth phase (Elling et al., 2014), oxygen concentrations, and ammonia oxidation rates as well as between different species (Qin et al., 2015; Elling et al., 2017; Hurley et al., 2016, 2018).

In contrast, pH and salinity variations likely have minimal effect on the intact polar GDGT composition (Wuchter et al., 2004; Elling et al., 2015). GDGTs produced by archaea other than marine Thaumarchaeota can also affect the TEX_{86}, and several indices have been proposed to assess these affects, such as the %GDGT-0 index and the Methane Index reflecting methanogenic or methanotrophic archaeal GDGT production, and the %GDGT$_{RS}$ index as a tool to identify Red Sea-type GDGT distributions (Zhang et al., 2011; Sinninghe Damsté et al., 2012; Inglis et al., 2015). Furthermore, it has been shown that input from the terrestrial environment can potentially affect the TEX_{86} proxy, which can be monitored by the branched isoprenoid tetraether (BIT) index (Hopmans et al., 2004), which is based upon the ratio of crenarchaeol, predominantly produced by marine Thaumarchaeota, and branched GDGTs (brGDGTs), which predominantly derive from the continent. Typically, BIT values <0.3 are considered to reflect marine conditions (e.g., Weijers et al., 2006; Zhu et al., 2011; Sinninghe Damsté, 2016).

The most recent lipid-based proxy for SST is the Long-chain Diol Index (LDI) based on the relative abundances of specific long-chain alkyl diols (LCDs), i.e., those with alcohol groups positioned at C-1 and at C-13 or C-15 (Supplementary Fig. S1). Analysis of marine surface sediments from all over the world showed a strong correlation of the LDI with SST (Rampen et al., 2012). Although this proxy has been applied successfully in several studies (e.g., Naafs et al., 2012; Lopes dos Santos et al., 2013; Smith et al., 2013; Plancq et al., 2015; Jonas et al., 2017), a lack of understanding still

complicates the application of this proxy. For instance, the source organisms are not well known. Whereas 1,13- and 1,15-diols have been observed in cultures of marine and freshwater eustigmatophyte microalgae (e.g., Volkman et al., 1992, 1999; Méjanelle et al., 2003; Rampen et al., 2014b), the observed LCD distributions are dissimilar to those observed in marine sediments, and therefore their role as LCD producers remains uncertain (Versteegh et al., 1997, 2000; Rampen et al., 2012, 2014b). Furthermore, riverine input into the marine realm might compromise the LDI (de Bar et al., 2016; Lattaud et al., 2017a, 2017b), while Rodrigo-Gámiz et al. (2015) obtained unrealistic LDI-derived SSTs due to high abundances of 1,14-diols, which are produced by *Proboscia* diatoms (Sinninghe Damsté et al., 2003; Rampen et al., 2014a), which also produce minor amounts of 1,13-diols. Saturated C_{28}, C_{30} and C_{32} 1,14-diols have also been observed in the marine Dictyochophyte *Apedinella radians* (Rampen et al., 2011), however, its importance as a 1,14-diol producer in the marine realm is unknown. In addition to LCDs, structurally corresponding long-chain keto-ols are also often observed and it has been proposed that these keto-ols are intermediate products of the oxidation of LCDs (Ferreira et al., 2001), although the chain length and positional isomer distributions for LCDs and keto-ols are not always similar (e.g., ten Haven et al., 1992; Yamamoto et al., 1996; Versteegh et al., 1997, 2000).

The TEX_{86}, $U_{37}^{K'}$ and LDI temperature proxies are all based upon the assumption that growth temperature is the main factor affecting the composition of the lipids on which they are based. However, many other factors, such as salinity, nutrient availability, inter- and intraspecies variation, may affect these proxies (e.g., Herbert, 2003; Qin et al., 2015; Elling et al., 2017). Importantly, application of these proxies in deep time, in particular the Cenozoic, implicitly assumes that the biological sources of these compounds have remained the same and that evolutionary ancestors of modern organisms producing these biomarkers responded in a similar way to temperature. However, for the $U_{37}^{K'}$ it has already been shown that its application is limited to the last ca. 55 Ma, due to the absence of tri-unsaturated LCAs in older sediments (Brassell, 2014 and References therein). Moreover, LCA distributions deviating from those in modern day sediments have been observed for Cretaceous and Paleocene sediments (Farrimond et al., 1986; Yamamoto et al., 1996; Brassell et al., 2004). Brassell (2014) assessed distributional variations in LCAs preserved in the sedimentary record with respect to changes in preserved calcareous nannoplankton over time and linked the alkenone distributions to evolutionary adaptations of the source organisms in response to climate change. However, this evaluation was done on sediments from multiple sites covering relatively short time periods and regions covering different climate zones. More importantly, proxies like the TEX_{86} and LDI have not been evaluated in a similar fashion, i.e., to assess the impact of (evolutionary) changes in the producers of GDGTs and LCDs, respectively, on the TEX_{86} and LDI proxies. In addition to evolutionary adaptations, diagenetic alterations may also influence lipids used for deriving paleoclimatic information.

In this study we investigated the lipid biomarker distributions in a sediment core from the New Jersey Shelf, USA, which covers the last 90 Myrs. These sediments were previously investigated by de Bar et al. (2019) for different temperature proxies, i.e., benthic foraminiferal stable oxygen isotopes ($\delta^{18}O$), Mg/Ca, clumped isotopes (Δ_{47}), MAT_{mrs} and TEX_{86} which showed that temperature reconstructions were consistent with each other. In this study we have examined in detail variations in distributions of LCAs, GDGTs and LCDs, which can give clues about changes in sources of these lipids compared to modern contributors. In particular, when biomarker lipids are encountered with unusual chain lengths com-

pared to modern day distributions in extant organisms and environments, this may hint at contributions of ancestral species which are different from today, although it is possible that different lipid distributions derive from the same species. Our results shed new light on the applicability of the biomarker lipids used for temperature reconstructions across the Mid- to Late Cretaceous and Cenozoic.

2. Materials and methods

2.1. Study site and age model

Lipid biomarkers were analyzed in sediments of the Bass River core (Ocean Drilling Program Leg 174AX, New Jersey Coastal Plain; 39°36′42″N, 74°26′12″W). A complete description of the core is provided by Miller et al. (1998). Nine sediment intervals spanning a time period of ca. 80 million years (Late Cretaceous to Late Miocene) were the subject of study, dated at ca. 91, 78, 74, 60, 50, 41, 33, 18 and 11 Ma, based on biostratigraphy, magnetostratigraphy, isotope stratigraphy and specific paleoclimatic events (for detailed description, see de Bar et al., 2019). Note that the age uncertainties are relatively large (in the order of millions of years), due to the coarse resolution of the age model. For every sediment interval, 10–15 subsamples (95 in total) were obtained, covering shorter time intervals (in the order of ten to hundreds of thousands of years) to assess short-term versus long-term variability.

2.2. Lipid extraction and analysis

Extracts of the sediments obtained by de Bar et al. (2019) were re-analyzed (see Supplementary Table S2 for the subsamples which were analyzed). In short, sediments were extracted via Accelerated Solvent Extraction (ASE) with dichloromethane (DCM)/methanol (MeOH) (9:1, v/v) and separated over Al_2O_3 into apolar, ketone and polar fractions, using n-hexane/DCM (9:1, v/v), n-hexane/DCM (1:1, v/v) and DCM/methanol (1:1, v/v), respectively. Fractions containing elemental sulfur were desulfurized using copper granules activated with 1 M HCL. Polar fractions were purified by polytetrafluoroethylene (PTFE) filtration (0.45 μm). A selection of alkenone fractions was further purified by chromatographic separation on silica impregnated with Ag^+, whereby DCM and ethyl acetate were used as eluents to purify the ketone fraction by removing saturated hydrocarbons (in the DCM fraction).

2.2.1. Long-chain alkenones

We analyzed the ketone fractions of between 2 and 13 samples per age interval for LCAs, depending on the presence of these compounds. The ketone fractions were re-dissolved in ethyl acetate prior to analysis. Quantification of the LCAs was achieved on an Agilent 6890N gas chromatograph (GC) with flame ionization detection (FID). Separation was achieved on a fused silica column with a length of 50 m and diameter of 0.32 mm, coated with a CP Sil-5 (thickness = 0.12 μm). Helium was used as carrier gas. The oven program was as follows: 70 °C at injection, increased by 20 °C/min to 200 °C followed by 3 °C/min until the final temperature of 320 °C. This end temperature was held for 30 min. The flow mode was a constant pressure of 100 kPa. Identification of the LCAs was performed on an Agilent 7890A GC coupled to an Agilent 5975C mass spectrometer (MS). The column, carrier gas, flow rate and oven program were identical to those described for GC–FID analysis but the end temperature was kept for 25 min, and the length of the column was 25 m instead of 50 m. The MS was operated at 70 eV, with an ion source temperature of 250 °C and an interface temperature of 320 °C. For both systems, injection was done on-column, with an injection volume of 1 μL. The mass spec-

tra of the LCAs were obtained in full scan mode, scanning between m/z 50 and 600 and compared with literature data (de Leeuw et al., 1980; Volkman et al., 1980; Marlowe et al., 1984). For the $C_{42:2}$ ketone, we could not detect the molecular ion mass (m/z 600), but its identification is based on the presence of the M^+-29 ion and its relative retention time. Since the $C_{38:2}$ methyl (Me) and ethyl (Et) ketones were not sufficiently separated on a CP Sil-5 column, complicating identification by GC–MS, one sample containing both isomers was also analyzed on an Agilent 7890B GC system equipped with a RTX200 column (mid-polarity) (cf. Longo et al., 2013) and FID. The RTX200 column had a length of 60 m, a diameter of 0.32 mm and a film thickness of 0.5 μm. The carrier gas was helium and the system was operated at a constant flow of 1.5 mL/min. The oven was programmed at 70 °C at injection, which was increased with a rate of 15 °C/min to 250 °C, followed by a linear gradient to 320 °C by 1.5 °C/min. This end temperature was held for 25 min. The injection volume was 1 μL. Comparison of the retention time with a sample containing $C_{38:2}$ Me confirmed the identity of this LCA in the Bass River sediment.

The $\delta^{13}C$ composition for the $C_{37:2}$ and $C_{38:2}$ LCAs of a sediment from the 41.2 Ma age interval, and of the $C_{40:2}$ LCA for the 77.8 Ma age interval was analyzed, by means of gas chromatography–isotope ratio mass spectrometry (GC–IRMS). Analyses were performed on a Thermo Delta V isotope ratio monitoring mass spectrometer coupled to a Thermo Trace 1310 GC. Separation was achieved on a column identical to that of the GC–FID but with a length of 25 m. The oven temperature at injection was 70 °C, which was then increased by 20 °C/min to 130 °C, followed by 4 °C/min to the end temperature of 320 °C at which it was held for 20 min. The $\delta^{13}C$ data represent averaged values of replicate analyses and are reported in delta notation relative to the VPDB standard using CO_2 reference gas calibrated to the NBS-22 reference material. The instrumental reproducibility was monitored by co-injection of deuterated n-alkane standards (C_{20} and C_{24} perdeuterated n-alkanes) with the samples. Injection volumes of the samples varied between 2 and 3 μL; injection volume for the n-alkane standards was 0.4 μL. Based on the quadruplicate injection of the n-alkane standards, the instrumental error is <0.4‰.

2.2.2. Glycerol dialkyl glycerol tetraethers

The polar fractions containing the GDGTs and related lipids were re-dissolved in hexane/isopropanol (99:1, v/v) and analyzed using high performance liquid chromatography–atmospheric pressure chemical ionization mass spectrometry (HPLC–APCI-MS) on an Agilent 1260 HPLC, equipped with automatic injector, coupled to a 6130 Agilent MSD and HP Chemstation software according to Hopmans et al. (2016). Separation of the GDGTs was achieved in normal phase using 2 silica BEH HILIC columns in series (150 mm × 2.1 mm; 1.7 μm; Waters Acquity) at a temperature of 25 °C. Compounds were isocratically eluted with 82% A and 18% B for the first 25 min, followed by a gradient to 35% B in 25 min and a linear gradient to 100% B in 30 min. A = hexane and B = hexane/isopropanol (90:10, v/v) and the flow rate was 0.2 mL/min. The conditions for the APCI-MS were identical to Schouten et al. (2007) and Hopmans et al. (2016). We assessed the distributions of GDGTs and related glycerol ether lipids by monitoring m/z 900–1400 rather than single ion monitoring as performed previously (de Bar et al., 2019) to investigate the distribution of ether lipids other than those used in the TEX_{86} and BIT proxies. The injection volume was 10 μL. For each age interval we analyzed three polar fractions (27 samples in total) on single quadrupole UHPLC–MS and integrated the extracted ion chromatograms of the protonated molecules for the ether lipids, with exception of the hydroxy GDGTs (OH-GDGTs) for which the $[M+H]^+$ – H_2O ions were integrated (Liu et al., 2012b, 2012c). The integrated peak area of iGDGT-4 was corrected for the contribution of the isotope peak of

crenarchaeol by subtracting 45% of the crenarchaeol peak (Hopmans et al., 2000; Pitcher et al., 2011). We report fractional abundances based on peak areas which were not corrected for possible differences in response factors between the various glycerol ether lipids.

For confirmation of the identity of the ether lipids, we performed UHPLC–high resolution MS (HRMS) on 1 to 2 samples per age interval, using an Agilent 1290 Infinity I equipped with thermostatted auto-injector and column compartment coupled to a Q Exactive (Quadrupole Orbitrap hybrid MS) MS equipped with ion max source with APCI probe (Thermo Fisher Scientific, USA). Positive-ion APCI setting were as follows: capillary temperature 200 °C, sheath gas (N_2) 50 arbitrary units (AU); vaporizer temperature 400 °C; auxiliary gas (N_2) 5 AU, corona current 2.5 μA, APCI heater temperature 400 °C; S-lens 100 V. Chromatography was identical as described above for the UHPLC–MS analyses (i.e., 2 silica BEH HILIC columns in series according to Hopmans et al., 2016). Ether lipids were analyzed with a mass range of m/z 600–2000 (resolution 70,000), followed by data-dependent MS^2 (resolution 17,500), in which the ten most abundant masses in the mass spectrum (with the exclusion of isotope peaks) were fragmented successively (stepped normalized collision energy 15, 20, 25; isolation window 1.0 Da). A dynamic exclusion window of 6 s, with a mass tolerance of 3 ppm, was applied. In addition, an inclusion list was used with a mass tolerance of 3 ppm, comprehensively targeting ether lipids described in the literature. Identification was achieved by comparison of exact mass and fragmentation spectra with literature data (e.g., Knappy et al., 2009; Liu et al., 2012a, 2012b, 2012c; Zhu et al., 2014; Naafs et al., 2018).

To assess the sources of branched GDGTs we calculated the #rings$_{tetra}$ index for the two youngest time intervals characterized by a BIT index >0.3, according to Sinninghe Damsté et al. (2016):

$$\#rings_{tetra} = ([brGDGT\ Ib] + 2 \times [brGDGT\ Ic])/([brGDGT\ Ia] + [brGDGT\ Ib] + [brGDGT\ Ic]) \quad (1)$$

We calculated the ring index of OH-GDGTs (Lü et al., 2015) based on the peak areas of the $[M+H]^+ – H_2O$ ions of OH-GDGTs:

$$RI\text{-}OH = ([OH\text{-}GDGT\text{-}1] + 2 \times [OH\text{-}GDGT\text{-}2])/([OH\text{-}GDGT\text{-}1] + [OH\text{-}GDGT\text{-}2]) \quad (2)$$

To assess Red Sea-type GDGT contributions we calculated the %GDGT$_{RS}$ ratio according to Inglis et al. (2015):

$$\%GDGT_{RS} = ([Cren'] / ([GDGT\text{-}0] + [Cren'])) \times 100 \quad (3)$$

Lastly, we calculated the $f_{Creń:Creń+Cren}$ as proposed by O'Brien et al. (2017) to identify anomalous GDGT distributions in Cretaceous sediments:

$$f_{Cren':Cren'+Cren} = ([Cren'] / [Cren] + [Cren']) \quad (4)$$

2.2.3. Long-chain diols and keto-ols

Polar fractions were dried in inserts under a stream of nitrogen and silylated by addition of BSTFA (N,O-*bis*(trimethylsilyl)trifluoroacetamide) and pyridine, and subsequent heating at 60 °C for 35 min. Subsequently, LCDs and corresponding keto-ols were analyzed on an Agilent 7890B GC system interfaced to a 7000C GC Triple Quadrupole MS operated in single MS mode, and a selection of samples was analyzed on an Agilent 7890B gas chromatograph coupled to an Agilent 5977A mass spectrometer. We analyzed on average 5 samples per age interval. The oven was programmed with a starting temperature of 70 °C, increased to 130 °C with a 20 °C/min rate, followed by a gradient of 4 °C/min to the end temperature of 320 °C, which was held for 15 min. Fractions were injected on-column with an injection volume of 1 μL. The GC was equipped with a fused silica column (25 m × 0.32 mm) coated with

CP Sil-5 (film thickness 0.12 μm). The flow rate was 2 mL/min; the carrier gas was helium, and the mass spectrometer was operated at 70 eV. The ion source had a temperature of 250 °C, and the interface temperature was 330 °C. Identification of all the LCDs and keto-ols was performed in full scan mode (m/z 50–800) by comparison with published mass spectra (e.g., Volkman et al., 1992; Versteegh et al., 1997). To assess distributional changes over time, ion chromatograms (EICs) with m/z 271, 285, 299, 313, 327, 341, 355 and 369, which are characteristic ion fragments formed by cleavage adjacent to the OTMSi groups (silylated hydroxyl groups) (Versteegh et al., 1997) were integrated. Similarly, for the long-chain keto-ols, distribution changes were assessed in full scan, i.e., quantification using mass chromatograms of their M^+-15 ions, i.e., m/z 453, 481, 509, 537, 565 and 593, as these were typically the most abundant characteristic fragment ions. Corrections for the relative contributions of the fragment ions to the total ion counts were made (9% and 3% for the LCDs and keto-ols, respectively). Typically, the LCDs and keto-ols were present in trace amounts in the older sediments.

LCDs are easier to identify than keto-ols since the characteristic fragments resulting from cleavage adjacent to the mid-chain OTMSi group are abundant, and hence, are relatively easily recognized in mass spectra. For long-chain keto-ols, the characteristic fragments associated with the position of the keto-group are much less dominant in the mass spectra, and therefore suffer more from background noise (de Leeuw et al., 1981; Versteegh et al., 1997). For mass spectral identification of the keto-ols we used the diagnostic mid-chain cleavage fragments (Versteegh et al., 1997), the M^+-15 ions, as well as m/z 130, which is a typical fragment for long-chain keto-ols, possibly formed after steps of TMSi rearrangement and subsequent McLafferty rearrangement (de Leeuw et al., 1981).

The LDI index and the fractional abundance of the C_{32} 1,15-diol were computed by using peak areas obtained by integration of appropriate peaks in SIM analysis (cf. Rampen et al., 2012; de Bar et al., 2016):

$$LDI = [C_{30}1,15\text{-}diol]/([C_{28}1,13\text{-}diol] + [C_{30}1,13\text{-}diol] + [C_{30}1,15\text{-}diol]) \quad (5)$$

LDI values were converted to SST values via the following equation:

$$SST = (LDI\text{-}0.095)/0.033 \quad (6)$$

$$FC_{32}1,15\text{-}diol = [C_{32}1,15\text{-}diol]/([C_{28}1,13\text{-}diol] + [C_{30}1,13\text{-}diol] + [C_{30}1,15\text{-}diol] + [C_{32}1,15\text{-}diol]) \quad (7)$$

Due to the higher sensitivity of SIM compared to full scan, LCDs which were below the limit of detection in full scan mode in some samples (and are thus not shown in Fig. 6), were just above the quantification limit in SIM, and could therefore be used for proxy calculation. For these proxy calculations, all sediment subsamples (on average 10 per age interval) were analyzed in SIM. The identities of the LCD isomers were affirmed by selected MRM analyses (de Bar et al., 2017), confirming that the fragments originate from LCDs.

3. Results and discussion

3.1. Long-chain alkenone distributions

We detected LCAs in sediments for the age intervals of 91, 78, 50, 41 and 33 Ma (e.g., Fig. 1), but not in the sediments of 74, 60, 18 and 11 Ma. The sediments for the intervals of 91, 50 and 33 Ma contain the di-unsaturated C_{37} methyl (Me) and C_{38} ethyl (Et) ketones (Fig. 2), and the sediments of 50 Ma also contain the
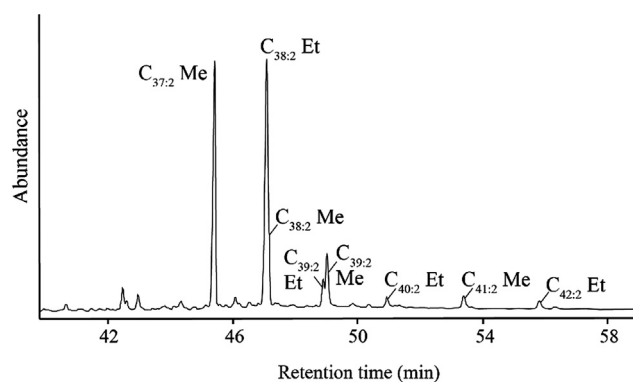
Fig. 1. Partial chromatogram of a ketone fraction of the extract from a sediment (ODP Leg 174AX) of ca. 41 Ma, illustrating the distribution of LCAs in the Bass River sediments. Separation was achieved using a CP Sil-5 column. Key: Et = ethyl ketone; Me = methyl ketone.

$C_{38:2}$ Me alkenone. The LCA abundance in these sediments is generally low, and particularly for the sediments of 33 and 91 Ma, the signal is around the detection limit. For the sediments of 78 Ma we observed the $C_{40:2}$ Et ketone as a dominant LCA in addition to the more commonly observed LCAs. In the sediments of 41 Ma the largest variety in LCAs was detected, i.e., the C_{37} Me, C_{38} Et and Me, C_{39} Et and Me, C_{40} Et, C_{41} Me and C_{42} Et di-unsaturated ketones (Fig. 2).

The absence of LCAs in the youngest sediment intervals, i.e., 11 and 18 Ma, can probably be explained by the nearshore depositional setting of the core site at that time, as revealed by the high BIT index (>0.8; de Bar et al., 2019), and thus the absence of marine LCA producers. One remarkable observation is that tri- or tetra-unsaturated LCAs were not detected in any of the studied sediments, indicating that the value for $U_{37}^{K'}$ was always 1.0. Brassell (2014) observed that tri-unsaturated LCAs, as well as the C_{38} di-unsaturated methyl ketone, only appeared in the sedimentary record after the Early Eocene Climatic Optimum (EECO; ± 52 Ma; Weller and Stein, 2008). The first evidence of tri-unsaturated LCAs in the sedimentary record was found in the Arctic Ocean immediately after the EECO. With time, there seems to be an equatorward migration of haptophytes able to produce tri-unsaturated LCAs, linked to reduced ocean warmth (Brassell, 2014), and the first occurrence of tri-unsaturated LCAs for the mid latitudes was around 45 Ma. Hence, for the Bass River site, we would expect the presence of tri-unsaturated LCAs for the age intervals of 33 and 41 Ma. Accordingly, the absence of the C_{37} tri-unsaturated LCAs in these sediments likely indicates SSTs >27 °C as above this temperature no tri-unsaturated LCAs are produced (e.g., Prahl and Wakeham, 1987; Volkman et al., 1995) rather than the absence of haptophyte populations producing tri-unsaturated LCAs. Indeed, for the time slice of 41 Ma, TEX_{86}^H indicates a temperature of 27 °C (de Bar et al., 2019), which would agree with a value of the $U_{37}^{K'}$ of 1.0. However, for the age interval of 33 Ma, the TEX_{86}^H-derived SST was 22 °C, which is inconsistent with the absence of tri-unsaturated LCAs. The reason for this is unclear, but one possibility is that TEX_{86}^H reflects subsurface temperatures (de Bar et al., 2019) and SST might have been much higher such that $U_{37}^{K'}$ nears unity. An alternative explanation for the absence of tri- and tetra-unsaturated LCAs may be diagenesis leading to selective degradation of LCAs with more double bonds (Hoefs et al., 1998).

Overall, the distributions observed for 33, 41 and 50 Ma are typical for marine haptophytes, such as the present-day *E. huxleyi* and *G. oceanica* (Volkman et al., 1980; Conte et al., 1995). However, present-day producers, i.e., *E. huxleyi* and *G. oceanica* evolved only
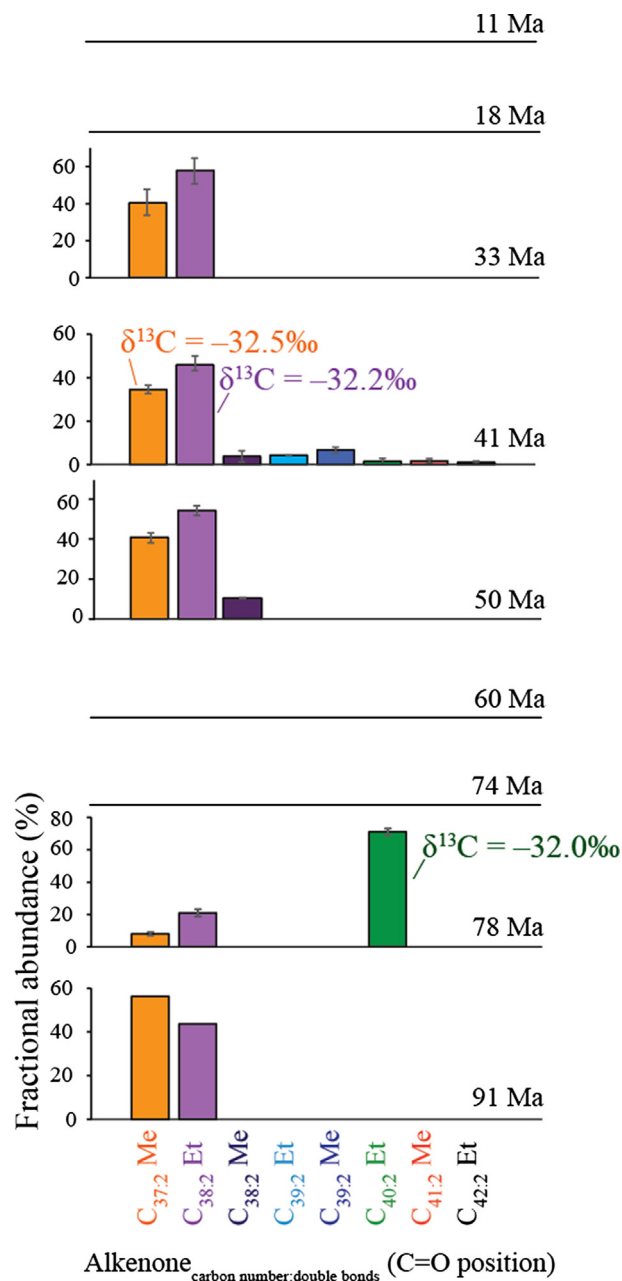

Fig. 2. LCA distributions through time for the Bass River record. Key: Et = ethyl ketone; Me = methyl ketone. Average fractional abundances (based on total summed LCAs for the specified time interval) are plotted, with error bars reflecting ±1σ standard deviations of the multiple sediments (*n* = 3–8) from one time slice analyzed. For the time slice 91 Ma, no error bars are provided since LCAs were only detected in one sediment sample.

290 kyrs and 1.85 Myrs ago, respectively (Pujos-Lamy, 1977; Thierstein et al., 1977; Raffi et al., 2006) and cannot be the source for the detected sedimentary LCAs. Since LCA distributions are similar to modern distributions up to the Eocene, it has been suggested that the most probable Cenozoic LCA producers are in the *Reticulofenestra* genus, which is part of the Noëlaerhabdaceae family (like *Emiliania* and *Gephyrocapsa*) (Marlowe et al., 1990). However, it is plausible that LCAs were also produced by any species within the three genera of Noëlaerhabdaceae, i.e., *Reticulofenestra*, *Dictyococcites* and *Cyclicargolithus* (Beltran et al., 2011; Plancq et al., 2012; Furota et al., 2016). In fact, for the late Oligocene-early Mio-

cene it was suggested that *Cyclicargolithus* was the main producer (Plancq et al., 2012).

The identification of the C_{38} Me ketone at 41 and 50 Ma is remarkable since it is not frequently reported (Brassell, 2014). For the Paleocene and Eocene, this LCA has only been detected in high-latitude sediments of the Arctic (ca. 44 Ma) (Weller and Stein, 2008) and the Iceland-Faeroe Ridge and Falkland Plateau (between ca. 39 and 28 Ma) (Dzvonik, 1996). In the sediments of 60 and 74 Ma, LCAs were not detected despite good preservation conditions for organic matter as evidenced by the presence of GDGTs and LCDs in the same sediments (see below). This potentially suggests that LCA producers were not present in the depositional environment.

At 78 Ma (Campanian), we observed an unusual LCA distribution with a highly dominant $C_{40:2}$ Et ketone. This LCA has solely been reported in Cretaceous (Farrimond et al., 1986; Brassell et al., 2004) and Danian sediments (Yamamoto et al., 1996). This unusual distribution suggests a different source organism for the LCAs as compared to those in younger sediments, or alternatively a separate biological source for the $C_{40:2}$ LCA. However, the stable carbon isotopic composition of the $C_{40:2}$ LCA ($-32.0 \pm 0.2‰$) is identical to the $\delta^{13}C$ values of the $C_{37:2}$ and $C_{38:2}$ LCAs ($-32.5 \pm 0.4‰$ and $-32.2 \pm 0.1‰$, respectively) measured for the age interval of 41 Ma. Factors which can impact the $\delta^{13}C$ of LCAs include growth rate, cell geometry and pCO_2 (Pagani, 2014 and References therein). Since pCO_2 was similar around 41 and 78 Ma (Foster et al., 2017) and environmental conditions were not dramatically different at our site, our results suggest that the $C_{40:2}$ LCA at 78 Ma was produced by haptophytes with similar cell dimensions and biosynthetic pathways as those producing C_{37} and C_{38} LCAs, but from a different family than Noëlaerhabdaceae. Nevertheless, the unusual Mesozoic LCA distributions suggests care should be taken in applying the $U_{37}^{K'}$ index to sediments from the early Cenozoic.

3.2. GDGTs and other ether lipids

In addition to the iGDGTs and brGDGTs used for the TEX_{86} and BIT indices, we have assessed distributional changes of all other ether lipids which were visible by scanning between m/z 900 and 1400, to evaluate potential relationships between these lipids and the GDGTs used in the proxies. For instance, transformation of iGDGTs into diagenetic products might potentially affect the applicability of the TEX_{86}. The ether lipid distributions revealed the presence of predominantly iGDGTs (15–67% of the total ether lipid assemblage) and brGDGTs (1–70%; Fig. 3). The two youngest time intervals (11 and 18 Ma) are characterized by relatively high amounts of brGDGTs (40–70%).

To constrain the sources of these branched GDGTs we calculated the #rings$_{tetra}$ index (Eq. (1)), the average number of cyclopentane moieties of the tetramethylated brGDGTs, which when >0.7 indicates that sources other than soil and rivers must contribute to the branched GDGT pool (Sinninghe Damsté, 2016). The #rings$_{tetra}$ index for these sediments range between 0.08 and 0.20, suggesting that the brGDGTs derive from a soil/riverine source, and not from in situ production in the shelf sediments (Sinninghe Damsté, 2016; Fig. 3). Accordingly, the BIT index indicates a mostly terrestrial signal for the two youngest time intervals (BIT index > 0.8).

The sediments of >33 Ma are dominated by iGDGTs, reflecting a mostly marine signal (BIT index < 0.3; de Bar et al., 2019). However, since the BIT index is a ratio, it is unclear whether this is due to reduced terrestrial input or increased archaeal productivity (e.g., Fietz et al., 2011). In addition to the commonly detected iGDGTs, GDGT-0 to GDGT-4, crenarchaeol (Sinninghe Damsté

et al., 2002), and its isomer (Cren′), trace amounts of GDGT-5 were tentatively identified in one of the sediments of the 18 Ma age interval (Fig. 3). Additionally, we detected a suite of other classes of ether lipids (see Supplementary Fig. S2 for lipid structures), some of which may derive from GDGTs by diagenesis.

Hydroxylated analogues of the iGDGTs (i.e., OH-GDGT-0, -1 and -2; Liu et al., 2012b, 2012c), were detected in the sediments of the time slices 18, 33 and 41 Ma, albeit in low relative abundances (0–1.1% fractional abundance; Fig. 3). Liu et al. (2012b, 2012c) showed the presence of OH-GDGTs in marine sediments, also solely with 0–2 cyclopentane moieties, whereas the iGDGT distributions comprise members with 0–3 cyclopentane moieties and crenarchaeol. Therefore, it was suggested that this potentially indicates different sources or different environmental conditions affecting the production of both groups of GDGTs.

The presence of, and number of rings in, OH-GDGTs in sediments has previously been linked to SST (Fietz et al., 2013) with relatively low amounts of OH-GDGTs at high SST, which is in agreement with our data. Lü et al. (2015) also observed a positive correlation between the weighted average number of cyclopentane moieties in OH-GDGT-1 and -2 (the RI-OH index; Eq. (2)) and SST. We obtained average RI-OH values of 1.4 and 1.7 for the time intervals of 33 and 41 Ma, respectively, corresponding to annual mean SSTs of ca. 17 °C and 29 °C, which compare reasonably well with the average TEX_{86}^{H}-derived SSTs of ca. 22 °C and 27 °C (de Bar et al., 2019). We observed positive correlations (although not significant; $R^2 = 0.84$ and 0.85) between the relative abundance of OH-GDGT-0 and -1 and iGDGT-0, suggesting related sources for these lipids at this site, while there was no correlation between the OH-GDGTs and the other iGDGTs.

Glycerol monoalkyl glycerol tetraethers (GMGTs; "H-shaped" GDGTs, Supplementary Fig. S2) are another group of glycerol ether lipids detected. The only iGMGT detected was iGMGT-0, present in low relative abundance (0.2–1.9%). iGMGTs have been reported in thermophilic archaea (e.g., Morii et al., 1998; Sugai et al., 2004; Schouten et al., 2008a; Knappy et al., 2009, 2011, 2015), the methanogenic archaeon *Methanothermus* (Koga and Morii, 2005), environmental samples (Schouten et al., 2008b; Liu et al., 2012c; Lincoln et al., 2013; Jaeschke et al., 2014), and recently also in peat bogs (Naafs et al., 2018). Schouten et al. (2008b) suggested that benthic archaea possibly produce this compound. BrGMGTs, the GMGT homologues of brGDGTs Ia, IIa and IIIa, were sometimes present in much higher relative abundances (0–19%). BrGMGT Ia was reported in several marine sediments (Liu et al., 2012c) and in the oxygen minimum zone of the Eastern Tropical North Pacific Ocean (Xie et al., 2014). Recently, Naafs et al. (2018) reported these three brGMGTs in peat bogs. The fractional abundances of the brGMGTs correlate ($R^2 = 0.3$–0.8) with those of the associated brGDGTs, indicating a terrestrial origin like the brGDGTs (Fig. 3), in agreement with the results of Naafs et al. (2018).

Glycerol dialkanol diether (GDD; Knappy and Keely, 2012; Liu et al., 2012a, 2012c) derivatives, i.e., GDGTs that have lost one glycerol unit (Supplementary Fig. S2), were also identified throughout the entire record (Fig. 3). The predominant GDDs are derivatives of the major GDGTs (iGDGT-0, crenarchaeol, brGDGT Ia), i.e., iGDD-0, iGDD-crenarchaeol (0–9% fractional abundance) and brGDD Ia (0–4%). Liu et al. (2012a, 2012c) observed that iGDDs and iGDGTs have similar ring distributions, suggesting similar origins, either indicating a biosynthetic relationship or due to diagenetic transformation. GDDs are observed both in their core lipid form as well as in their IPL form in archaeal cultures (Elling et al., 2014, 2015, 2017; Meador et al., 2014), suggesting a biosynthetic origin. However, Yang et al. (2014) observed an exponential decrease in the GDGT/(GDGT + GDD) ratio with depth in a Chinese loess-paleosol sequence, which indicates that GDDs have a diagenetic origin. In
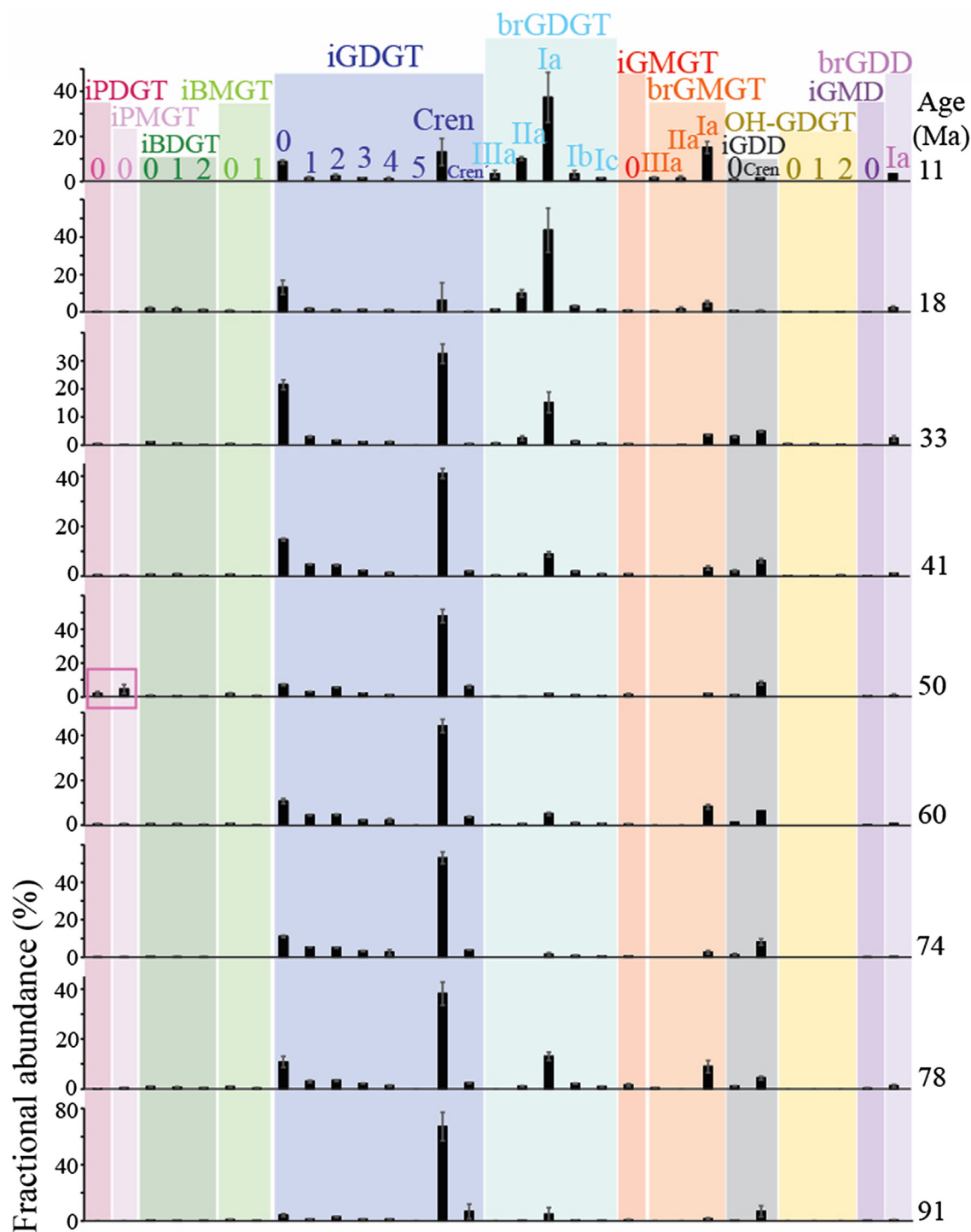
Fig. 3. Glycerol ether lipid distributions through time for the Bass River record. The bars reflect the fractional abundances of the glycerol ether lipids (based on total summed glycerol ether lipids for the specified time interval); the error bars reflect ±1σ standard deviation of three sediment samples analyzed per time interval. The pink box in the 50 Ma age interval highlights the occurrence of iPDGTs. (For interpretation of the references to colour in this figure legend, the reader is referred to the web version of this article.)

agreement, we observed a significant positive relation between the fractional abundance of iGDD-0 and iGDGT-0, and iGDD-Cren and Crenarchaeol ($R^2 = 0.64$ and 0.41, respectively; p-values < 0.001), as well as between the branched GDD Ia and branched GDGT Ia ($R^2 = 0.69$; p-value < 0.001).

Interestingly, the isoprenoidal glycerol monoalkanediol diether-0 (iGMD-0; Bauersachs and Schwark, 2016; Liu et al., 2016) is present in all studied time intervals except for the youngest interval. If

indeed iGDD-0 and iGDD-Cren (partially) result from the diagenetic transformation of GDGT-0 and crenarchaeol, respectively, this could potentially compromise the TEX$_{86}$ proxy. Therefore, we cross-correlated the ratio of crenarchaeol over the sum of crenarchaeol and iGDGT-0 with the same ratio for their iGDD counterparts, shown in Fig. 4. The evidently strong positive correlation between these two ratios ($R^2 = 0.98$; slope ~ 1 and intercept ~ 0; $p < 0.001$; $n = 23$) suggests that, if indeed the iGDDs are degrada-
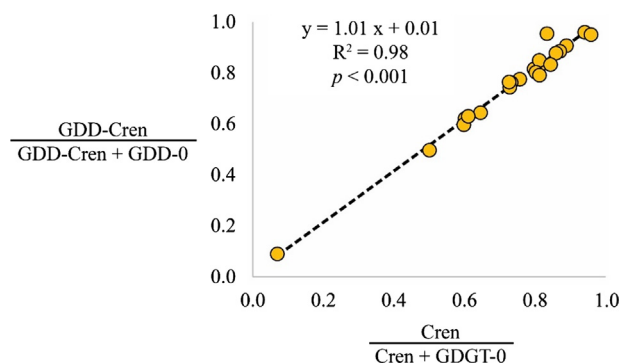
Fig. 4. Cross-correlation of the ratio of crenarchaeol over the sum of crenarchaeol and GDGT-0 versus the same ratio for the GDD-counterparts for the examined sediments from the Bass River record.

tion products, the diagenetic conversion of iGDGT-0 and crenarchaeol into iGDD-0 and iGDD-Cren is proportional. Assuming similar degradation dynamics hold for the iGDGTs used in the TEX_{86}, this suggests that degradation does not affect the distribution of iGDGTs and, hence, of TEX_{86} values.

Some less common tetraethers, where one of the glycerol moieties is replaced by another group, were also detected; butanetriol dibiphytanyl glycerol tetraether-0, -1 and -2 (iBDGT-0, -1, -2; 0–5.8% fractional abundance) and the pentanetriol dibiphytanyl glycerol tetraether-0 (iPDGT-0; 0–2.6%). These lipids were recently identified in marine and estuarine sediments (Zhu et al., 2014) as well as in the methanogenic archaeon *Methanomassiliicoccus luminyensis* (Becker et al., 2016). The iBDGTs were detected in relatively low abundance (0–6%) throughout the entire Bass River record with exception of the youngest sediment interval (11 Ma; Fig. 3). iPDGT-0 was present in relatively small amounts (0–3%), except for the youngest and oldest time interval (11 and 91 Ma; Fig. 3). It showed a relatively high abundance (1.6%) in the time interval of 50 Ma (Fig. 3), together with a novel tentatively identified ether lipid (Supplementary Fig. S3), the isoprenoidal pentanetriol monoalkyl glycerol tetraether-0 (iPMGT-0; 3.9%).

Similarly, we tentatively identified (Supplementary Fig. S4) the isoprenoidal butanetriol monoalkyl glycerol tetraether-0 and -1 (iBMGT-0 and -1; 0–2.2%; Fig. 3), which were detected in the same sediments as the iBDGTs. These tentative identifications were based on retention times, the exact protonated molecular mass obtained by HRMS and its MS^2 fragmentation pattern (Supplementary Figs. S3 and S4). The fractional abundances of iBMGT-1 and iGMGT-0 reveal a very strong positive relation with each other ($R^2 = 0.83$; $p < 0.001$). iBMGT-0 strongly correlates with iPDGT-0, iPMGT-0 and iGMD-0 ($R^2 = 0.76$, 0.83 and 0.76, respectively; p-values < 0.001), suggesting similar sources. Interestingly, the fractional abundance of the iBDGTs does not correlate with the abundance of these lipids.

Overall, despite the wide structural variety in glycerol ether lipids detected throughout Bass River over the last ca. 90 Myrs, the distributions of the main iGDGTs stayed relatively similar from 33 to 91 Ma and they remained the most abundant glycerol ether lipids (Fig. 3). This suggests a similar biological source throughout this time interval and no major diagenetic transformations. iGDDs were encountered in the record but they remained minor relative to the iGDGTs and their formation does not seem to affect the iGDGT distribution. Potential secondary effects on the TEX_{86}^H were assessed by de Bar et al. (2019) by means of calculation of the Methane Index, the %GDGT-0 and Ring Index, which were all below recommended threshold values. Additionally, we calculated here the %GDGT$_{RS}$ (Eq. (3)) to identify Red Sea-type GDGT distributions, since it is known to differ from other modern ocean settings (Inglis

et al., 2015). For the time intervals where TEX_{86} SST < 30 °C, the % GDGT$_{RS}$ is always below the threshold, i.e. <30. Additionally, we applied the $f_{Creń:Creń+Cren}$ as proposed by O'Brien et al. (2017) (Eq. (4)), to identify anomalous GDGT distributions in Cretaceous sediments, associated with $f_{Creń:Creń+Cren}$ values of >0.25. However, all values for the Bass River are <0.16.

The observed distributional changes of the iGDGTs appear to relate to temperature changes as TEX_{86}-derived SSTs correlate well with SST estimates based on other temperature proxies determined on the same sediments (de Bar et al., 2019), as well as with the global benthic oxygen isotopic compilation (Zachos et al., 2008; Friedrich et al., 2012). This indicates that the fundamental principles underlying the TEX_{86} proxy relationship with temperature potentially remained the same over the last ca. 90 Myrs. iGDGTs have been found in sediments up to 140 Ma (Kuypers et al., 2001; Carrillo-Hernandez et al., 2003; Jenkyns et al., 2012), and recently even in Early Jurassic sediments (ca. 191 Ma; Robinson et al., 2017), and based on genetic analysis it was estimated that Thaumarchaeota originated more than 1 Gyr ago (Blank, 2009; Spang et al., 2010). Moreover, the same temperature adaptation, i.e., an increase in the number of cyclopentane rings with increasing temperature, as observed with the TEX_{86} has also been evidenced for distantly related hyperthermophilic archaea (see Schouten et al., 2013 and References therein), signifying that this adaptation mechanism is shared by more archaeal phyla and thus likely also the ancestors of modern day Thaumarchaeota.

3.3. Long-chain diol and keto-ol distributions

All sediment intervals contained LCDs (e.g., Fig. 5 for a sediment of 50 Myrs old), albeit generally in low amounts. Particularly, for the age intervals of 11, 60, 74 and 91 Ma, the LCDs identified were often near the detection limit. The two youngest time intervals investigated (i.e., ca. 11 and 18 Ma) reveal C_{30} and C_{32} 1,15-diols as dominant LCDs (Fig. 6; Supplementary Table S1). Sediments with the ages of 33, 41 and 50 Ma reveal different LCD distributions with the dominant isomers being the C_{26} 1,13-, C_{28} 1,12-, C_{30} 1,15-, C_{32} 1,15- and C_{34} 1,17-diol. Plancq et al. (2014) reported similar LCD distributions for Eocene-Oligocene (ca. 31–37 Ma) sediments of DSDP Site 511 in the South Atlantic as observed here for the 33 and 41 Ma age intervals (i.e., the C_{26} 1,12–1,13- and 1,14-diol, C_{28} 1,12-, 1,13-, 1,14-diol and C_{30} 1,13- and 1,14-diol). In the sediments of 60 Ma, the C_{28} 1,12-diol, C_{30} 1,15-diol and the C_{30} 1,12-diol were detected of which the C_{28} 1,12-diol occurs in the highest abundance. For the interval of 74 Ma, the C_{26} 1,13-, C_{28} 1,12-, 1,13- and 1,14-diols and the C_{30} 1,15-diol were detected, of which the C_{26} 1,13-diol was the most abundant. In the sediments of 78 and 91 Ma, we solely detected the C_{26} 1,13-diol. Through time, there is a clear gradual shift in chain length dominance towards shorter chain lengths from C_{32} to C_{26} (Fig. 6).

We also quantified long-chain keto-ols, suspected diagenetic products of LCDs (e.g., Ferreira et al., 2001). The concentrations in the youngest time interval (11 Ma) were too low for unambiguous identification of keto-ols. For the interval of 18 Ma, we detected the C_{30} and C_{32} 1,15-keto-ols in addition to the C_{34} 1,15-keto-ol, and trace abundances the C_{36} 1,19-keto-ol (Fig. 6). The polar fractions of the sediments of 33 Ma generally contained higher backgrounds, complicating identifications of keto-ols, and consequently we solely unambiguously identified the C_{32} 1,15-keto-ol. Further back in time, the presence of the C_{28} 1,12- and C_{26} 1,13-keto-ols was established (Fig. 6).

Overall, the long-chain keto-ols show a gradual shift in chain length through time, similar to that observed for the LCDs (from C_{32} to C_{26}) (Fig. 6), which would agree with the idea that long-chain keto-ols result from oxidation of the mid-chain alcohol group of the LCDs (Ferreira et al., 2001). Another possibility is that the
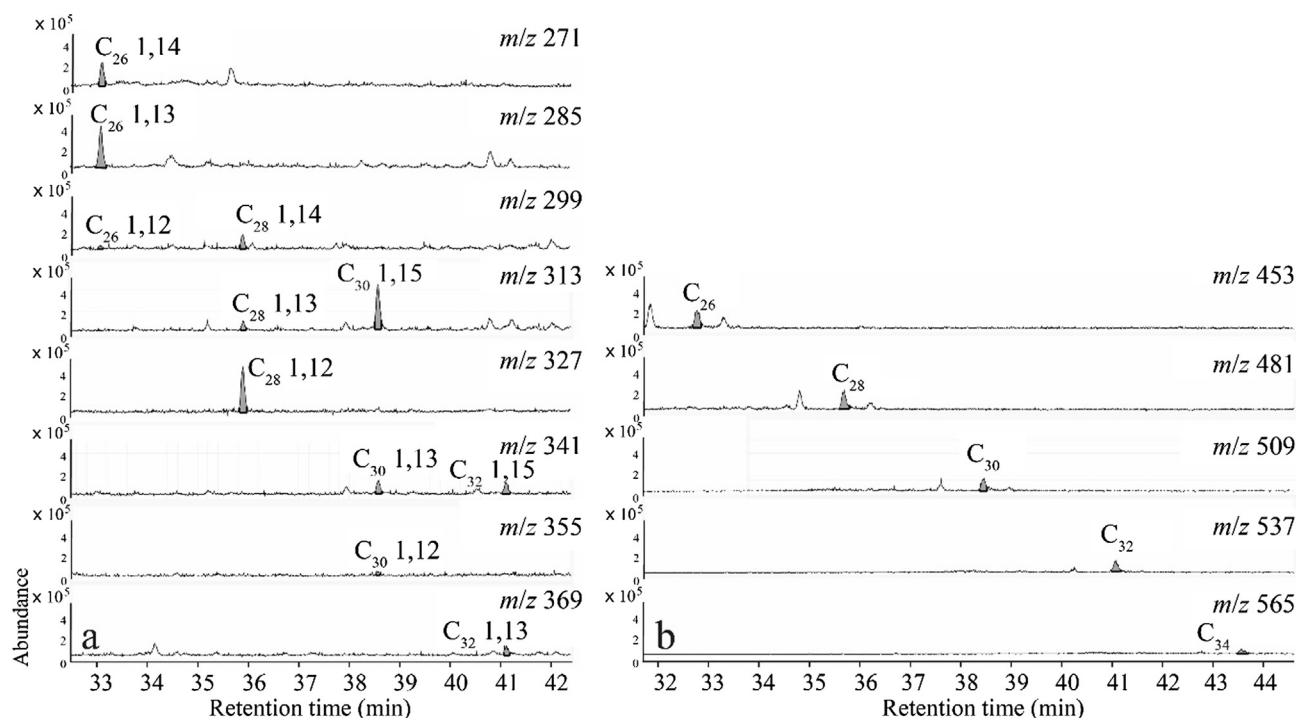
Fig. 5. Partial extracted ion chromatograms revealing the presence of LCDs (a) and long-chain keto-ols (b) present in a Bass River sediment of 50 Ma (ODP Leg 174AX). For quantification of the LCDs, the fragment ions formed by cleavage adjacent to the OTMSi groups (silylated hydroxyl groups) were integrated, whereas for keto-ols the M$^+$-15 ions (M$^+$–CH$_3$) were used.

keto-ols are biosynthesized by the same algae producing LCDs, but evidence for this is lacking. We did not recognize keto-ols for all corresponding LCDs, but keto-ols were generally present in trace amounts, and the characteristic fragment ions related to the position of the keto-group, on which the identification of the keto-ols are based, have relatively low abundances (de Leeuw et al., 1981) which prohibited unambiguous identifications of all keto-ols.

Particularly interesting are the C$_{28}$ 1,12- and C$_{26}$ 1,13- and 1,14-LCDs, which become more dominant in the older sediment intervals. The C$_{28}$ 1,12-diol has been previously observed in lake sediments (Shimokawara et al., 2010; Rampen et al., 2014a), in trace amounts in cultures of the eustigmatophyte freshwater algae *Vischeria* spp. (Volkman et al., 1999; Rampen et al., 2014a), and marine *Proboscia* diatoms (Rampen et al., 2007). Additionally, low abundances were observed in marine sediments from the Bransfield Basin (Holocene; Antarctic Peninsula; Willmott et al., 2010), the Arabian Sea (recent; Rampen et al., 2007), the Oman margin (Pliocene; ten Haven and Rullkötter, 1991), and the Chilean margin (Late Quaternary; de Bar et al., 2018). Interestingly, all these sediments were deposited under upwelling conditions, and contained high relative abundances of 1,14-diols (produced by *Proboscia* diatoms; Sinninghe Damsté et al., 2003; Rampen et al., 2014b).

Since the C$_{28}$ 1,12-diol has also been detected in *Proboscia* cultures, albeit in relatively low abundances, the *Proboscia* diatoms are likely to be the present-day producer of the C$_{28}$ 1,12-diol in the marine realm. The relative high abundance of the C$_{28}$ 1,12-diol in the sediments from ca. 33 to 74 Ma, may therefore indicate the dominance of a diatom population closely related to *Proboscia*. In addition to the C$_{28}$ 1,12-diol, the C$_{26}$ 1,14- and 1,13-diols are relatively dominant between 91 and 33 Ma. In the two oldest sediment intervals (91 and 78 Ma) only the C$_{26}$ 1,13-diol was detected. Similar to the C$_{28}$ 1,12-diol, these LCDs are generally not observed in high abundance in recent marine sediments. Moreover, to the best of our knowledge, they have only been reported

for sediments of Lake Baikal (Japan; Shimokawara et al., 2010), Holocene sapropels in the Mediterranean (ten Haven et al., 1987) and, in trace amounts, in *Proboscia* cultures (Rampen et al., 2007). Accordingly, this latter observation might indicate that these LCDs were (as for the C$_{28}$ 1,12-diol) produced by a group of diatoms closely related to *Proboscia*. However, the observed co-occurrence of the C$_{28}$ 1,12-/C$_{26}$ 1,13-diols with their corresponding keto-ols would imply that *Proboscia,* or related diatoms, are not the source of these lipids, since 1,14-keto-ols are generally not detected in modern sediments in contrast to 1,13- and 1,15-keto-ols (e.g., Versteegh et al., 1997; Sinninghe Damsté et al., 2003). Similarly, for this site, we did not detect 1,14-keto-ols.

Sinninghe Damsté et al. (2003) hypothesized that because *Proboscia* diatoms sink relatively fast to the seafloor, and the lipids are protected by a silica frustule, the 1,14-diols are much less exposed to oxygen in the water column, preventing the oxidation of 1,14-diols. In contrast, 1,13- and 1,15-diols are likely longer exposed to oxygen and therefore degraded to 1,13- and 1,15-keto-ols. In agreement with this idea, we have not detected the C$_{29}$ 12-hydroxy methyl alkanoate in the Bass River sediments, a typical biomarker for *Proboscia* and potentially formed from common precursors (C$_{28}$ 12-hydroxy fatty acid) as the 1,14-diols (Sinninghe Damsté et al., 2003).

Interestingly, Yamamoto et al. (1996) observed similar LCD distributions for Danian sediments (Geulhemmerberg; the Netherlands; ca. 65 Ma): the C$_{26}$ 1,13-, C$_{28}$ 1,12- and 1,13-, C$_{30}$ 1,13- and 1,15- and C$_{32}$ 1,15-diols, suggesting that the rarely reported C$_{26}$ 1,13- and C$_{28}$ 1,12-diols may have been more common in the early Cenozoic. However, they observed different keto-ol distributions, i.e., the C$_{32}$ 1,15-, C$_{34}$ 1,13- and 1,15- and C$_{36}$ 1,15-keto-ols. This discrepancy in LCD and keto-ol distribution might be the result of different settling speeds of material with which the LCDs are associated, due to different producers, and thus different oxygen exposure times. The authors did detect the C$_{28}$ 12-hydroxy fatty
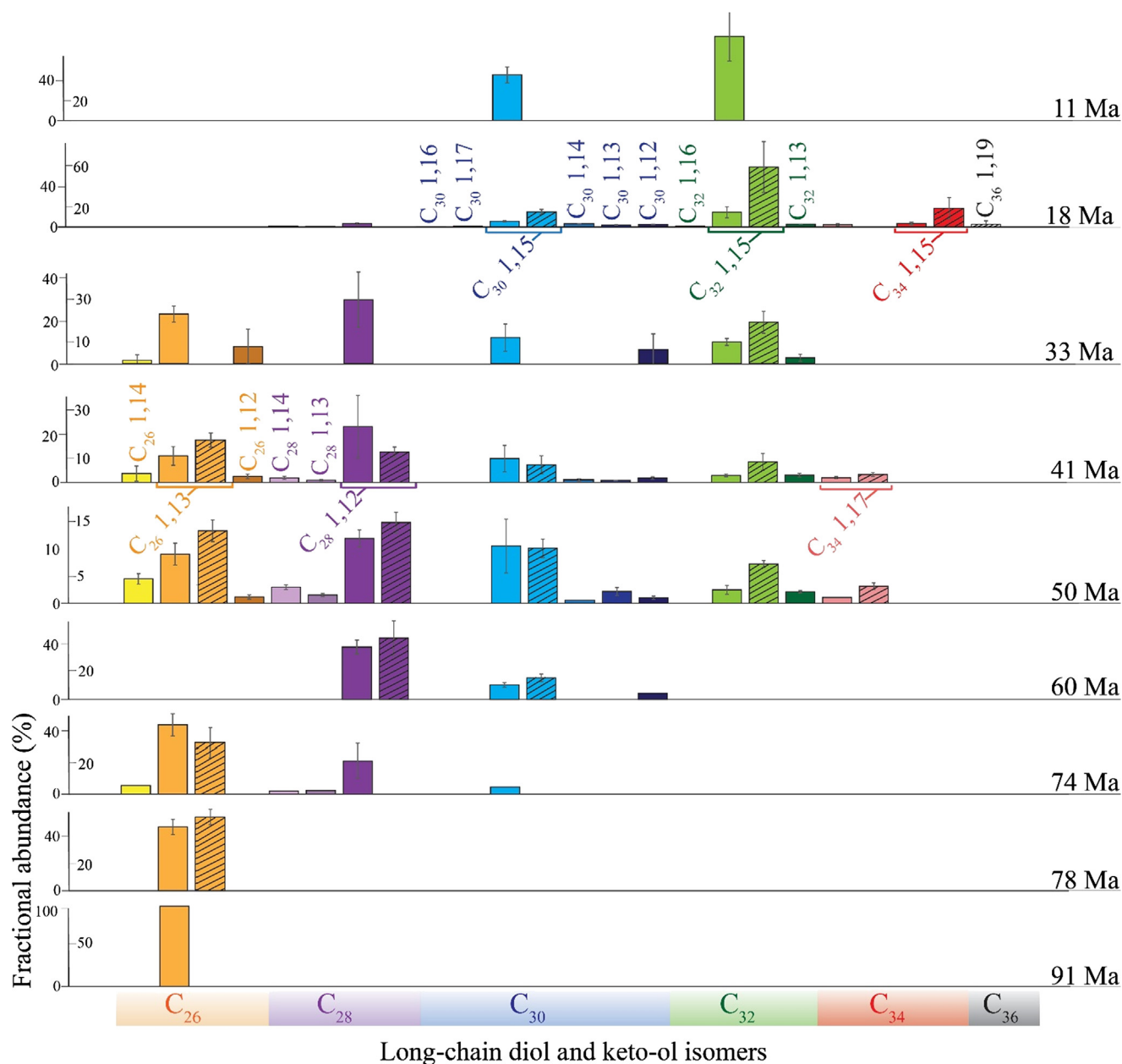
Fig. 6. LCD and keto-ol distributions through time for the Bass River record. Keto-ols are plotted right next to the associated LCD isomers, highlighted by a dashed pattern. Bars represent average fractional abundances (based on summed LCD and long-chain keto-ol abundance) for the specified time intervals. Error bars reflect ±1σ standard deviations of the different sediments of a particular age interval. When there is no error bar, the LCD or keto-ol was identified in solely one sediment sample for that time interval.

acid at their site, which is an indication that, in contrast to the Bass River, the C_{28} 1,12- and C_{26} 1,13-diols were potentially produced by diatoms closely related to *Proboscia*.

Integrating these long-term LCD distribution changes with fossil distributions or molecular phylogenic data, which can give insight in the evolution of organisms, could potentially shed light on the source organisms of LCDs. However, little is known on the evolutionary history of the present-day LCD producers, i.e., the eustigmatophytes (1,13- and 1,15-diols), *Proboscia* diatoms (1,14-diols) and the dictyochophyte *Apedinella radians* (1,14-diols). Molecular clock analysis estimated the divergence of different genera within the Eustigmatophyceae and Dictyochophyceae families to have most likely occurred around 120 and 280 Ma, respectively (Brown and Sorhannus, 2010), i.e., predating our oldest sedimentary LCD occurrence (±91 Ma).

Proboscia taxa originate from a centric diatom lineage which likely evolved between approximately 149 and 125 Ma (Sorhannus, 2007). Indeed, a number of fossil *Proboscia* species has been reported for the Cenozoic and the Late Cretaceous despite their weak preservation potential (Jordan and Priddle, 1991; Koç et al., 2001; Jordan and Ito, 2002). The oldest reported occurrences of preserved *Proboscia* is for Late Cretaceous sediments, for which in total six species were described (Hajós and Stradner, 1975; Harwood and Nikolaev, 1995; Jordan and Ito, 2002), suggesting that diversification within the *Proboscia* genus already occurred prior to the Late Cretaceous. Jordan and Ito (2002) argued, based on morphological grounds and the absence of *Proboscia* fossils in Early Cretaceous sediments (Gersonde and Harwood, 1990), that a possible ancestor would be the *Kreagra* diatom genus, observed in Early Cretaceous sediments. Thus, the present-day producers

of the most dominant LCDs all evolved prior to our oldest LCD occurrence. The observed trends may therefore be predominantly explained by shifting populations of *Proboscia*, causing a shift to shorter chain lengths with increasing sediment deposition age.

Values for the LDI (Eq. (5)), the paleothermometer based on LCDs, could be calculated for the five younger time intervals (i.e., 11, 18, 33, 41 and 50 Ma; Fig. 7a). For sediments older than 50 Ma, solely the C_{28} 1,13-diol was tentatively identified in trace amounts in a sediment from 74 Ma, but the C_{30} 1,13-diol could not be unambiguously identified, implying that for this site, the applicability of the LDI is restricted to the last ± 50 Myrs. However, Yamamoto et al. (1996) reported low amounts of the C_{30} 1,13-diol for Danian sediments (±66 Ma) suggesting that the LDI might be applicable in older sediments at other sites.

The LDI-derived SSTs vary between ca. 15 and 22 °C (Fig. 7a). The SST trend does not agree with that of the other temperature records for this site (i.e., $\delta^{18}O$ bottom water temperature (BWT), the TEX_{86}^H SST and MAT_{mrs} mean air temperatures (MAT) as reported by de Bar et al., 2019; Fig. 7a). LDI-derived SSTs are ca. 2 °C and 14 °C lower as compared to the TEX_{86}^H-derived SSTs and they show only a subtle increase in SST from 50 to 41 Ma (ca. 1.5 °C), whereas other proxy records, as well as the global benthic $\delta^{18}O$ compilation, show a strong cooling after the Early Eocene Climatic Optimum (EECO).

Rodrigo-Gámiz et al. (2015) previously reported LDI values for surface sediments around Iceland, in which the 1,13- and 1,15-diols were relatively low compared to the 1,14-diols. They obtained LDI-SSTs which were significantly lower compared to satellite SSTs, and they proposed that the *Proboscia* diatoms might be at least a partial source of the 1,13- and 1,15-diols in that region, affecting the LDI. Likely, the LDI signal we obtained for the Bass River site is similarly affected by 1,13- and 1,15-diols produced by unknown organisms producing the more abundant C_{28} 1,12- and C_{26} 1,13-diols.

We also determined the fractional abundance of the C_{32} 1,15-diol (Eq. (7)), which is a potential indicator of riverine organic matter input (de Bar et al., 2016; Lattaud et al., 2017a, 2017b). We observed a good correlation between the BIT index, a proxy for soil and riverine input (e.g., Weijers et al., 2007; Zell et al., 2014; de Jonge et al., 2015), and the fractional abundance of the C_{32} 1,15-diol ($R^2 = 0.72$, p-value < 0.001; $n = 38$; Fig. 7b), suggesting a contribution of terrestrially derived organic carbon, potentially providing an alternative explanation for the erroneous LDI SSTs (cf. de Bar et al., 2016). So far, the C_{32} 1,15-diol as tracer for contribution of riverine organic carbon has only been tested for Late Quaternary records (Lattaud et al., 2017b; Jonas et al., 2017; Warnock et al., 2017). The agreement between the fractional abundance of the C_{32} 1,15-diol and the BIT index determined for the Bass River site over the last ca. 50 Myrs suggests that this proxy might also be applicable over longer timescales.

4. Conclusions

In this study we have assessed changes in lipid biomarker distributions (LCAs, GDGTs, LCDs, keto-ols) in the Bass River core (New Jersey shelf, North Atlantic) from the late Cretaceous to the Pliocene to gain insight into the long-term evolution of sources of these lipid biomarkers and associated temperature proxies and potential effects of diagenesis. Tri-unsaturated LCAs were absent, and consequently the $U_{37}^{K'}$ results in reconstructed SSTs >27 °C for the Mid-Eocene and later. At 78 Ma, we observed a highly dominant $C_{40:2}$ Et ketone, potentially suggesting different ancestors and thereby limiting the applicability of the $U_{37}^{K'}$ to the Cenozoic. However, the stable carbon isotopic composition is highly similar to that of the $C_{37:2}$ and $C_{38:2}$ LCAs of the age interval of 41 Ma,
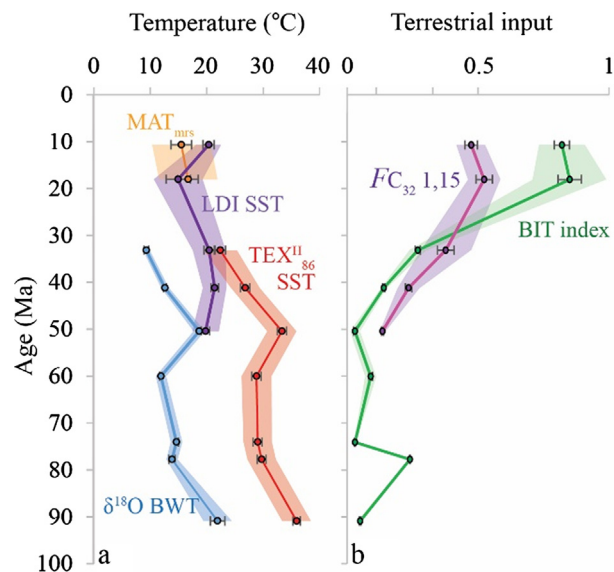

Fig. 7. Proxy records for the Bass River site based on LCDs. (a) The LDI SST record plotted together with TEX_{86}^H-derived SSTs, MAT_{mrs} air temperatures and $\delta^{18}O$-derived BWTs adapted from de Bar et al. (2019). The transparent envelopes represent propagations of short-term variability within the age interval and calibration errors of the proxies. The error bars reflect the standard errors ($\sigma/\sqrt{n}$, where σ = standard deviation, reflecting the short-term variability and n = number of sediment samples); when not visible, the error bars are smaller than the symbol size. (b) The BIT index (from de Bar et al., 2019) and the fractional abundance of the C_{32} 1,15-diol. Transparent envelopes here reflect standard deviation from the mean for the respective age intervals; the error bars reflect the standard errors.

potentially suggesting similar sources. We have encountered a wide variety of glycerol ether lipids, and tentatively identified three new GMGT homologues of previously reported isoprenoid PDGTs and BDGTs, i.e., iPMGT-0 and iBMGT-0 and -1. The iGDGT distributions observed throughout the core are highly comparable to distributions typically observed in marine Thaumarchaeota and in present-day sediments, suggesting that the fundamental principles underlying the relation of the TEX_{86}^H proxy to temperature remained consistent back to ±91 Ma. We also detected GDDs, which have a diagenetic or biosynthetic origin. If they are formed by diagenetic conversion of GDGTs, this conversion appears to be constant through time, implying there is no effect of degradation on the TEX_{86} proxy. The LDI could solely be calculated for sediments up to ca. 50 Ma, due to the absence of 1,13-diols in the older sediment intervals and calculated temperatures and trend did not agree with other records. Changing LCD distributions were observed with time, revealing the dominant C_{28} 1,12-diol and C_{26} 1,13-diol between 33 and 91 Ma which may have impacted the LDI. Good agreement between the fractional abundance of the C_{32} 1,15-diol and the BIT index over the last 50 Myrs suggesting that this proxy for riverine input is potentially applicable up to the Eocene. Long-chain keto-ols had the same isomer distributions as the LCDs suggesting a diagenetic link.

Appendix A. Supplementary material

Supplementary data to this article can be found online at https://doi.org/10.1016/j.orggeochem.2018.12.005.

*Associate Editor—**Ann Pearson***

References

Basse, A., Zhu, C., Versteegh, G.J.M., Fischer, G., Hinrichs, K.-U., Mollenhauer, G., 2014. Distribution of intact and core tetraether lipids in water column profiles of suspended particulate matter off Cape Blanc, NW Africa. Organic Geochemistry 72, 1–13.

Bauersachs, T., Schwark, L., 2016. Glycerol monoalkanediol diethers: a novel series of archaeal lipids detected in hydrothermal environments. Rapid Communications in Mass Spectrometry 30 (581), 54–60.

Becker, K.W., Elling, F.J., Yoshinaga, M.Y., Söllinger, A., Urich, T., Hinrichs, K.-U., 2016. Unusual butane- and pentanetriol-based tetraether lipids in *Methanomassiliicoccus luminyensis*, a representative of the seventh order of methanogens. Applied and Environmental Microbiology 82, 4505–4516.

Beltran, C., Flores, J.A., Sicre, M.A., Baudin, F., Renard, M., de Rafelis, M., 2011. Long chain alkenones in the Early Pliocene Sicilian sediments (Trubi Formation - Punta di Maiata section): Implications for the alkenone paleothermometry. Palaeogeography, Palaeoclimatology, Palaeoecology 308, 253–263.

Bijl, P.K., Schouten, S., Sluijs, A., Reichart, G.-J., Zachos, J.C., Brinkhuis, H., 2009. Early Palaeogene temperature evolution of the southwest Pacific Ocean. Nature 461, 776–779.

Blank, C.E., 2009. Not so old Archaea - the antiquity of biogeochemical processes in the archaeal domain of life. Geobiology 7, 495–514.

Brassell, S.C., Eglinton, G., Marlowe, I.T., Pflaumann, U., Sarnthein, M., 1986. Molecular stratigraphy – a new tool for climatic assessment. Nature 320, 129–133.

Brassell, S.C., Dumitrescu, M., Shipboard Party, O.D.P., 2004. Recognition of alkenones in a lower Aptian porcellanite from the west-central Pacific. Organic Geochemistry 35, 181–188.

Brassell, S.C., 2014. Climatic influences on the Paleogene evolution of alkenones. Paleoceanography 29, 255–272.

Brocks, J.J., Pearson, A., 2005. Building the biomarker tree of life. In: Banfield, J.E., CerviniSilva, J., Nealson, K.H. (Eds.), Reviews in Mineralogy & Geochemistry, vol. 59, pp. 233–258.

Brown, J.W., Sorhannus, U., 2010. A molecular genetic timescale for the diversification of autotrophic stramenopiles (Ochrophyta): substantive underestimation of putative fossil ages. PLoS One 5, (9). https://doi.org/10.1371/journal.pone.0012759 e12759.

Carrillo-Hernandez, T., Schaeffer, P., Adam, P., Albrecht, P., Derenne, S., Largeau, C., 2003. Remarkably well-preserved archaeal and bacterial membrane lipids in 140 million years old sediment from the Russian platform (Kasphpir oil shales, Upper Jurassic). In: 21st International Meeting on Organic Geochemistry2003, Krakow Part 1, pp. 77–78 (Abstract).

Chen, W., Mohtadi, M., Schefuss, E., Mollenhauer, G., 2014. Organic-geochemical proxies of sea surface temperature in surface sediments of the tropical eastern Indian Ocean. Deep-Sea Research I 88, 17–29.

Conte, M.H., Thompson, A., Eglinton, G., Green, J.C., 1995. Lipid biomarker diversity in the coccolithophorid *Emiliania huxleyi* (Prymnesiophyceae) and the related species *Gephyrocapsa oceanica*. Journal of Phycology 31, 272–282.

Conte, M.H., Sicre, M.-A., Ruhlemann, C., Weber, J.C., Schulte, S., Schulz-Bull, D., Blanz, T., 2006. Global temperature calibration of the alkenone unsaturation index ($U_{37}^{K'}$) in surface waters and comparison with surface sediments. Geochemistry Geophysics Geosystems 7 (2), Q02005. https://doi.org/10.1029/2005GC001054.

de Bar, M.W., Dorhout, D.J.C., Hopmans, E.C., Rampen, S.W., Sinninghe Damsté, J.S., Schouten, S., 2016. Constraints on the application of long chain diol proxies in the Iberian Atlantic margin. Organic Geochemistry 101, 184–195.

de Bar, M.W., Hopmans, E.C., Verweij, M., Dorhout, D.J.C., Sinninghe Damsté, J.S., Schouten, S., 2017. Development and comparison of chromatographic methods for the analysis of long chain diols and alkenones in biological materials and sediment. Journal of Chromatography A 1521, 150–160.

de Bar, M.W., Stolwijk, D.J., McManus, J.F., Sinninghe Damsté, J.S., Schouten, S., 2018. A Late Quaternary climate record based on long-chain diol proxies from the Chilean margin. Climate of the Past 14, 1783–1803.

de Bar, M.W., de Nooijer, L.J., Schouten, S., Ziegler, M., Sluijs, A., Reichart, G.-J., 2019. Comparing sea water temperature proxy records for the past 90 Myrs from the shallow shelf record Bass River, New Jersey. Paleoceanography and Paleoclimatology

de Jonge, C., Stadnitskaia, A., Hopmans, E.C., Cherkashov, G., Fedotov, A., Streletskaya, I.D., Vasiliev, A.A., Sinninghe Damsté, J.S., 2015. Drastic changes in the distribution of branched tetraether lipids in suspended matter and sediments from the Yenisei River and Kara Sea (Siberia): implications for the use of brGDGT-based proxies in coastal marine sediments. Geochimica et Cosmochimica Acta 165, 200–225.

de Leeuw, J.W., van der Meer, F.W., Rijpstra, W.I.C., Schenck, P.A., 1980. On the occurrence and structural identification of long chain unsaturated ketones and hydrocarbons in sediments. Physics and Chemistry of the Earth 12, 211–217.

de Leeuw, J.W., Rijpstra, W.I.C., Schenck, P.A., 1981. The occurrence and identification of C_{30}, C_{31} and C_{32} alkan-1,15-diols and alkan-15-one-1-ols in Unit I and Unit II Black Sea sediments. Geochimica et Cosmochimica Acta 45, 2281–2285.

Dzvonik, J.P., 1996. Alkenones as Records of Oceanic Paleotemperatures; Studies of Eocene and Oligocene Sediments from the North, South, and Equatorial Atlantic. Indiana University at Bloomington, Bloomington, IN, USA, p. 21.

Elling, F.J., Könneke, M., Lipp, J.S., Becker, K.W., Gagen, E.J., Hinrichs, K.-U., 2014. Effects of growth phase on the membrane lipid composition of the thaumarchaeon *Nitrosopumilus maritimus* and their implications for archaeal lipid distributions in the marine environment. Geochimica et Cosmochimica Acta 141, 579–597.

Elling, F.J., Könneke, M., Mussmann, M., Greve, A., Hinrichs, K.-U., 2015. Influence of temperature, pH, and salinity on membrane lipid composition and TEX$_{86}$ of marine planktonic thaumarchaeal isolates. Geochimica et Cosmochimica Acta 171, 238–255.

Elling, F.J., Könneke, M., Nicol, G.W., Stieglmeier, M., Bayer, B., Spieck, E., de la Torre, J.R., Becker, K.W., Thomm, M., Prosser, J.I., Herndl, G.J., Schleper, C., Hinrichs, K.-U., 2017. Chemotaxonomic characterisation of the thaumarchaeal lipidome. Environmental Microbiology 19, 2681–2700.

Farrimond, P., Eglinton, G., Brassell, S.C., 1986. Alkenones in Cretaceous black shales, Blake-Bahama Basin, western North Atlantic. Organic Geochemistry 10, 897–903.

Ferreira, A.M., Miranda, A., Caetano, M., Baas, M., Vale, C., Sinninghe Damsté, J.S., 2001. Formation of mid-chain alkane keto-ols by post-depositional oxidation of mid-chain diols in Mediterranean sapropels. Organic Geochemistry 32, 271–276.

Fietz, S., Martinez-Garcia, A., Huguet, C., Rueda, G., Rosell-Melé, A., 2011. Constraints in the application of the Branched and Isoprenoid Tetraether index as a terrestrial input proxy. Journal of Geophysical Research – Oceans 116, C10032. https://doi.org/10.1029/2011JC007062.

Fietz, S., Huguet, C., Rueda, G., Hambach, B., Rosell-Melé, A., 2013. Hydroxylated isoprenoidal GDGTs in the Nordic Seas. Marine Chemistry 152, 1–10.

Forster, A., Schouten, S., Baas, M., Sinninghe Damsté, J.S., 2007a. Mid-Cretaceous (Albian-Santonian) sea surface temperature record of the tropical Atlantic Ocean. Geology 35, 919–922.

Forster, A., Schouten, S., Moriya, K., Wilson, P.A., Sinninghe Damsté, J.S., 2007b. Tropical warming and intermittent cooling during the Cenomanian/Turonian oceanic anoxic event 2: sea surface temperature records from the equatorial Atlantic. Paleoceanography 22, PA1219. https://doi.org/10.1029/2006PA001349.

Foster, G.L., Royer, D.L., Lunt, D.J., 2017. Future climate forcing potentially without precedent in the last 420 million years. Nature Communications 8. https://doi.org/10.1038/ncomms14845.

Friedrich, O., Norris, R.D., Erbacher, J., 2012. Evolution of middle to Late Cretaceous oceans – a 55 m.y. record of Earth's temperature and carbon cycle. Geology 40, 107–110.

Furota, S., Nakamura, H., Sawada, K., 2016. Long-chain alkenones and related distinctive compounds in the late Miocene and Pliocene sediments from the Gulf of Cadiz, eastern North Atlantic. Organic Geochemistry 101, 166–175.

Gersonde, R., Harwood, D.M., 1990. Lower Cretaceous diatoms from ODP Leg 113, Site 693 (Weddell Sea). Part 1: vegetative cells. In: Barker, P.F., Kennett, J.P., O'Connell, S., Pisias, N.G. (Eds.), Proceedings of the Ocean Drilling Program, Scientific Results, vol. 113. Ocean Drilling Program, College Station, Texas, pp. 365–402.

Hajós, M., Stradner, H., 1975. Late Cretaceous Archaeomonadaceae, Diatomaceae, and Silicoflagellatae from the South Pacific Ocean, Deep Sea Drilling Project, Leg 29, Site 275. Initial Reports of the Deep Sea Drilling Project 29, 913–1009.

Harwood, D., Nikolaev, V., 1995. Cretaceous Diatoms: Morphology, Taxonomy, Biostratigraphy. In: Blome, C.D., Whalen, P.M., Reed, K.M. (Eds.), Siliceous Microfossils: Paleontological Society Short Courses in Paleontology, 8. Paleontology Society. University of Tennessee, Knoxville, Tennessee, pp. 81–106.

Herbert, T.D., 2003. Alkenone paleotemperature determinations. In: Holland, H.D., Turekian, K.K. (Eds.), Treatise on Geochemistry, vol. 6. The Oceans and Marine Geochemistry, pp. 391–432.

Ho, S.L., Mollenhauer, G., Fietz, S., Martinez-Garcia, A., Lamy, F., Rueda, G., Schipper, K., Meheust, M., Rosell-Melé, A., Stein, R., Tiedemann, R., 2014. Appraisal of TEX86 and TEX86L thermometries in subpolar and polar regions. Geochimica et Cosmochimica Acta 131, 213–226.

Hoefs, M.J.L., Versteegh, G.J.M., Rijpstra, W.I.C., de Leeuw, J.W., Sinninghe Damsté, J.S., 1998. Postdepositional oxic degradation of alkenones: Implications for the measurement of palaeo sea surface temperatures. Paleoceanography 13, 42–49.

Hollis, C.J., Taylor, K.W.R., Handley, L., Pancost, R.D., Huber, M., Creech, J.B., Hines, B.R., Crouch, E.M., Morgans, H.E.G., Crampton, J.S., Gibbs, S., Pearson, P.N., Zachos, J.C., 2012. Early Paleogene temperature history of the Southwest Pacific Ocean: reconciling proxies and models. Earth and Planetary Science Letters 349, 53–66.

Hopmans, E.C., Schouten, S., Pancost, R.D., van der Meer, M.T.J., Sinninghe Damsté, J.S., 2000. Analysis of intact tetraether lipids in archaeal cell material and

sediments by high performance liquid chromatography/atmospheric pressure chemical ionization mass spectrometry. Rapid Communications in Mass Spectrometry 14, 585–589.

Hopmans, E.C., Weijers, J.W.H., Schefuss, E., Herfort, L., Sinninghe Damsté, J.S., Schouten, S., 2004. A novel proxy for terrestrial organic matter in sediments based on branched and isoprenoid tetraether lipids. Earth and Planetary Science Letters 224, 107–116.

Hopmans, E.C., Schouten, S., Sinninghe Damsté, J.S., 2016. The effect of improved chromatography on GDGT-based palaeoproxies. Organic Geochemistry 93, 1–6.

Huguet, C., Schimmelmann, A., Thunell, R., Lourens, L.J., Sinninghe Damsté, J.S., Schouten, S., 2007. A study of the TEX$_{86}$ paleothermometer in the water column and sediments of the Santa Barbara Basin, California. Paleoceanography 22, PA3203. https://doi.org/10.1029/2006PA001310.

Hurley, S.J., Elling, F.J., Könneke, M., Buchwald, C., Wankel, S.D., Santoro, A.E., Lipp, J. S., Hinrichs, K.-U., Pearson, A., 2016. Influence of ammonia oxidation rate on thaumarchaeal lipid composition and the TEX$_{86}$ temperature proxy. Proceedings of the National Academy of Sciences of the United State of America 113, 7762–7767.

Hurley, S.J., Lipp, J.S., Close, H.G., Hinrichs, K.-U., Pearson, A., 2018. Distribution and export of isoprenoid tetraether lipids in suspended particulate matter from the water column of the Western Atlantic Ocean. Organic Geochemistry 116, 90–102.

Inglis, G.N., Farnsworth, A., Lunt, D., Foster, G.L., Hollis, C.J., Pagani, M., Jardine, P.E., Pearson, P.N., Markwick, P., Galsworthy, A.M.J., Raynham, L., Taylor, K.W., Pancost, R.D., 2015. Descent toward the Icehouse: eocene sea surface cooling inferred from GDGT distributions. Paleoceanography 30, 1000–1020.

Jaeschke, A., Eickmann, B., Lang, S.Q., Bernasconi, S.M., Strauss, H., Fruh-Green, G.L., 2014. Biosignatures in chimney structures and sediment from the Loki's Castle low-temperature hydrothermal vent field at the Arctic Mid-Ocean Ridge. Extremophiles 18, 545–560.

Jenkyns, H.C., Schouten-Huibers, L., Schouten, S., Sinninghe Damsté, J.S., 2012. Warm Middle Jurassic-Early Cretaceous high-latitude sea-surface temperatures from the Southern Ocean. Climate of the Past 8, 215–226.

Jordan, R.W., Priddle, J., 1991. Fossil members of the diatom genus *Proboscia*. Diatom Research 6, 55–61.

Jordan, R., Ito, R., 2002. Observations on *Proboscia* species from Late Cretaceous sediments, and their possible evolution from *Kreagra*. In: John, J. (Ed.), Proceedings of the 15th International Diatom Symposium. ARG Gantner Verlag KG, Ruggell, Liechtenstein, pp. 313–329.

Jonas, A.-S., Schwark, L., Bauersachs, T., 2017. Late Quaternary water temperature variations of the Northwest Pacific based on the lipid paleothermometers TEX$_{86}^H$, $U_{37}^{K'}$ and LDI. Deep Sea Research Part I: Oceanographic Research Papers 125, 81–93.

Kim, J.-H., Schouten, S., Hopmans, E.C., Donner, B., Sinninghe Damsté, J.S., 2008. Global sediment core-top calibration of the TEX$_{86}$ paleothermometer in the ocean. Geochimica et Cosmochimica Acta 72, 1154–1173.

Kim, J.-H., Crosta, X., Michel, E., Schouten, S., Duprat, J., Sinninghe Damsté, J.S., 2009. Impact of lateral transport on organic proxies in the Southern Ocean. Quaternary Research 71, 246–250.

Kim, J.-H., van der Meer, J., Schouten, S., Helmke, P., Willmott, V., Sangiorgi, F., Koç, N., Hopmans, E.C., Sinninghe Damsté, J.S., 2010. New indices and calibrations derived from the distribution of crenarchaeal isoprenoid tetraether lipids: Implications for past sea surface temperature reconstructions. Geochimica et Cosmochimica Acta 74, 4639–4654.

Kim, J.-H., Crosta, X., Willmott, V., Renssen, H., Bonnin, J., Helmke, P., Schouten, S., Sinninghe Damsté, J.S., 2012. Holocene subsurface temperature variability in the eastern Antarctic continental margin. Geophysical Research Letters 39, L06705. https://doi.org/10.1029/2012GL051157.

Kim, J.-H., Villanueva, L., Zell, C., Sinninghe Damsté, J.S., 2016. Biological source and provenance of deep-water derived isoprenoid tetraether lipids along the Portuguese continental margin. Geochimica et Cosmochimica Acta 172, 177–204.

Knappy, C.S., Chong, J.P.J., Keely, B.J., 2009. Rapid discrimination of archaeal tetraether lipid cores by liquid chromatography–tandem mass spectrometry. Journal of the American Society for Mass Spectrometry 20, 51–59.

Knappy, C.S., Nunn, C.E.M., Morgan, H.W., Keely, B.J., 2011. The major lipid cores of the archaeon *Ignisphaera aggregans*: implications for the phylogeny and biosynthesis of glycerol monoalkyl glycerol tetraether isoprenoid lipids. Extremophiles 15, 517–528.

Knappy, C.S., Keely, B.J., 2012. Novel glycerol dialkanol triols in sediments: transformation products of glycerol dibiphytanyl glycerol tetraether lipids or biosynthetic intermediates? Chemical Communications 48, 841–843.

Knappy, C., Barillà, D., Chong, J., Hodgson, D., Morgan, H., Suleman, M., Tan, C., Yao, P., Keely, B., 2015. Mono-, di- and trimethylated homologues of isoprenoid tetraether lipid cores in archaea and environmental samples: mass spectrometric identification and significance. Journal of Mass Spectrometry 50, 1420–1432.

Koç, N., Labeyrie, L., Manthé, S., Flower, B.P., Hodell, D.A., Aksu, A., 2001. The last occurrence of *Proboscia curvirostris* in the North Atlantic marine isotope stages 9–8. Marine Micropaleontology 41, 9–23.

Koga, Y., Morii, H., 2005. Recent advances in structural research on ether lipids from archaea including comparative and physiological aspects. Bioscience Biotechnology and Biochemistry 69, 2019–2034.

Koga, Y., Morii, H., 2007. Biosynthesis of ether-type polar lipids in Archaea and evolutionary considerations. Microbiology and Molecular Biology Reviews 71, 97–120.

Kuypers, M.M.M., Blokker, P., Erbacher, J., Kinkel, H., Pancost, R.D., Schouten, S., Sinninghe Damsté, J.S., 2001. Massive expansion of marine archaea during a mid-Cretaceous oceanic anoxic event. Science 293, 92–94.

Lattaud, J., Kim, J.-H., de Jonge, C., Zell, C., Sinninghe Damsté, J.S., Schouten, S., 2017a. The C$_{32}$ alkane-1,15-diol as a tracer for riverine input in coastal seas. Geochimica et Cosmochimica Acta 202, 146–158.

Lattaud, J., Dorhout, D., Schulz, H., Castañeda, I.S., Sinninghe Damsté, J.S., Schouten, S., 2017b. The C$_{32}$ alkane-1,15-diol as a proxy of late Quaternary riverine input in coastal margins. Climate of the Past 13, 1049–1061.

Lee, K.E., Kim, J.-H., Wilke, I., Helmke, P., Schouten, S., 2008. A study of the alkenone, TEX$_{86}$, and planktonic foraminifera in the Benguela Upwelling System: implications for past sea surface temperature estimates. Geochemistry Geophysics Geosystems 9, Q10019. https://doi.org/10.1029/2008GC002056.

Lincoln, S.A., Bradley, A.S., Newman, S.A., Summons, R.E., 2013. Archaeal and bacterial glycerol dialkyl glycerol tetraether lipids in chimneys of the Lost City Hydrothermal Field. Organic Geochemistry 60, 45–53.

Linnert, C., Robinson, S.A., Lees, J.A., Bown, P.R., Pérez-Rodríguez, I., Petrizzo, M.R., Falzoni, F., Littler, K., Arz, J.A., Russell, E.E., 2014. Evidence for global cooling in the Late Cretaceous. Nature Communications 5. https://doi.org/10.1038/ncomms5194.

Littler, K., Robinson, S.A., Bown, P.R., Nederbragt, A.J., Pancost, R.D., 2011. High sea-surface temperatures during the Early Cretaceous Epoch. Nature Geoscience 4, 169–172.

Liu, Z.H., Pagani, M., Zinniker, D., DeConto, R., Huber, M., Brinkhuis, H., Shah, S.R., Leckie, R.M., Pearson, A., 2009. Global cooling during the Eocene-Oligocene climate transition. Science 323, 1187–1190.

Liu, X.-L., Lipp, J.S., Schröder, J.M., Summons, R.E., Hinrichs, K.-U., 2012a. Isoprenoid glycerol dialkanol diethers: A series of novel archaeal lipids in marine sediments. Organic Geochemistry 43, 50–55.

Liu, X.-L., Lipp, J.S., Simpson, J.H., Lin, Y.-S., Summons, R.E., Hinrichs, K.-U., 2012b. Mono- and dihydroxyl glycerol dibiphytanyl glycerol tetraethers in marine sediments: Identification of both core and intact polar lipid forms. Geochimica et Cosmochimica Acta 89, 102–115.

Liu, X.L., Summons, R.E., Hinrichs, K.-U., 2012c. Extending the known range of glycerol ether lipids in the environment: structural assignments based on tandem mass spectral fragmentation patterns. Rapid Communications in Mass Spectrometry 26, 2295–2302.

Liu, X.L., Birgel, D., Elling, F.J., Sutton, P.A., Lipp, J.S., Zhu, R., Zhang, C., Könneke, M., Peckmann, J., Rowland, S.J., Summons, R.E., Hinrichs, K.-U., 2016. From ether to acid: a plausible degradation pathway of glycerol dialkyl glycerol tetraethers. Geochimica et Cosmochimica Acta 183, 138–152.

Longo, W.M., Dillon, J.T., Tarozo, R., Salacup, J.M., Huang, Y.S., 2013. Unprecedented separation of long chain alkenones from gas chromatography with a poly (trifluoropropylmethylsiloxane) stationary phase. Organic Geochemistry 65, 94–102.

Lopes dos Santos, R.A.L., Prange, M., Castañeda, I.S., Schefuss, E., Mulitza, S., Schulz, M., Niedermeyer, E.M., Sinninghe Damsté, J.S., Schouten, S., 2010. Glacial-interglacial variability in Atlantic meridional overturning circulation and thermocline adjustments in the tropical North Atlantic. Earth and Planetary Science Letters 300, 407–414.

Lopes dos Santos, R.A.L., Spooner, M.I., Barrows, T.T., de Deckker, P., Sinninghe Damsté, J.S., Schouten, S., 2013. Comparison of organic ($U_{37}^{K'}$, TEX$_{86}^H$, LDI) and faunal proxies (foraminiferal assemblages) for reconstruction of late Quaternary sea surface temperature variability from offshore southeastern Australia. Paleoceanography 28, 377–387.

Lü, X.X., Liu, X.L., Elling, F.J., Yang, H., Xie, S.C., Song, J.M., Li, X.G., Yuan, H.M., Li, N., Hinrichs, K.-U., 2015. Hydroxylated isoprenoid GDGTs in Chinese coastal seas and their potential as a paleotemperature proxy for mid-to-low latitude marginal seas. Organic Geochemistry 89–90, 31–43.

Luo, G., Yang, H., Algeo, T.J., Hallmann, C., Xie, S., 2018. Lipid biomarkers for the reconstruction of deep-time environmental conditions. Earth-Science Reviews. https://doi.org/10.1016/j.earscirev.2018.03.005.

Marlowe, I.T., Brassell, S.C., Eglinton, G., Green, J.C., 1984. Long chain unsaturated ketones and esters in living algae and marine sediments. Organic Geochemistry 6, 135–141.

Marlowe, I.T., Brassell, S.C., Eglinton, G., Green, J.C., 1990. Long-chain alkenones and alkyl alkenoates and the fossil coccolith record of marine sediments. Chemical Geology 88, 349–375.

Meador, T.B., Zhu, C., Elling, F.J., Könneke, M., Hinrichs, K.-U., 2014. Identification of isoprenoid glycosidic glycerol dibiphytanol diethers and indications for their biosynthetic origin. Organic Geochemistry 69, 70–75.

Méjanelle, L., Sanchez-Gargallo, A., Bentaleb, I., Grimalt, J.O., 2003. Long chain *n*-alkyl diols, hydroxy ketones and sterols in a marine eustigmatophyte, *Nannochloropsis gaditana*, and in *Brachionus plicatilis* feeding on the algae. Organic Geochemistry 34, 527–538.

Miller, K.G., Sugarman, P.J., Browning, J.V., Olsson, R.K., Pekar, S.F., Reilly, T.J., Cramer, B.S., Aubry, M.-P., Lawrence, R.P., Curran, J., Stewart, M., Metzger, J.M., Uptegrove, J., Bukry, D., Burckle, L.H., Wright, J.D., Feigenson, M.D., Brenner, G.J., Dalton, R.F., 1998. Bass River Site. Proceedings of the Ocean Drilling Program, Initial Reports, 915 vol. 174AX.

Mollenhauer, G., Eglinton, T.I., Hopmans, E.C., Sinninghe Damsté, J.S., 2008. A radiocarbon-based assessment of the preservation characteristics of crenarchaeol and alkenones from continental margin sediments. Organic Geochemistry 39, 1039–1045.

Morii, H., Eguchi, T., Nishihara, M., Kakinuma, K., König, H., Koga, Y., 1998. A novel ether core lipid with H-shaped C$_{80}$-isoprenoid hydrocarbon chain from the

hyperthermophilic methanogen *Methanothermus fervidus*. Biochimica et Biophysica Acta - Lipids and Lipid Metabolism 1390, 339–345.

Müller, P.J., Kirst, G., Ruhland, G., von Storch, I., Rosell-Melé, A., 1998. Calibration of the alkenone paleotemperature index $U_{37}^{K'}$ based on core-tops from the eastern South Atlantic and the global ocean (60°N-60°S). Geochimica et Cosmochimica Acta 62, 1757–1772.

Naafs, B.D.A., Hefter, J., Stein, R., 2012. Application of the long chain diol index (LDI) paleothermometer to the early Pleistocene (MIS 96). Organic Geochemistry 49, 83–85.

Naafs, B.D.A., McCormick, D., Inglis, G.N., Pancost, R.D., 2018. Archaeal and bacterial H-GDGTs are abundant in peat and their relative abundance is positively correlated with temperature. Geochimica et Cosmochimica Acta 227, 156–170.

O'Brien, C.L., Robinson, S.A., Pancost, R.D., Sinninghe Damsté, J.S., Schouten, S., Lunt, D.J., Alsenz, H., Bornemann, A., Bottini, C., Brassell, S.C., Farnsworth, A., Forster, A., Huber, B.T., Inglis, G.N., Jenkyns, H.C., Linnert, C., Littler, K., Markwick, P., McAnena, A., Mutterlose, J., Naafs, B.D.A., Puttmann, W., Sluijs, A., van Helmond, N., Vellekoop, J., Wagner, T., Wrobel, N.E., 2017. Cretaceous sea-surface temperature evolution: constraints from TEX$_{86}$ and planktonic foraminiferal oxygen isotopes. Earth-Science Reviews 172, 224–247.

Ohkouchi, N., Eglinton, T.I., Keigwin, L.D., Hayes, J.M., 2002. Spatial and temporal offsets between proxy records in a sediment drift. Science 298, 1224–1227.

Pagani, M., 2014. Holland, Heinrich D Biomarker-based inferences of past climate: the alkenone pCO$_2$ proxy. In: Turekian, K.K. (Ed.), Treatise on Geochemistry. second ed. Elsevier, Oxford, pp. 361–378.

Pitcher, A., Hopmans, E.C., Mosier, A.C., Park, S.-J., Rhee, S.-K., Francis, C.A., Schouten, S., Sinninghe Damsté, J.S., 2011. Core and intact polar glycerol dibiphytanyl glycerol tetraether lipids of ammonia-oxidizing archaea enriched from marine and estuarine sediments. Applied and Environmental Microbiology 77, 3468–3477.

Plancq, J., Grossi, V., Henderiks, J., Simon, L., Mattioli, E., 2012. Alkenone producers during late Oligocene-early Miocene revisited. Paleoceanography 27, PA1202.

Plancq, J., Mattioli, E., Pittet, B., Simon, L., Grossi, V., 2014. Productivity and sea-surface temperature changes recorded during the late Eocene-early Oligocene at DSDP Site 511 (South Atlantic). Palaeogeography, Palaeoclimatology, Palaeoecology 407, 34–44.

Plancq, J., Grossi, V., Pittet, B., Huguet, C., Rosell-Melé, A., Mattioli, E., 2015. Multi-proxy constraints on sapropel formation during the late Pliocene of central Mediterranean (southwest Sicily). Earth and Planetary Science Letters 420, 30–44.

Prahl, F.G., Wakeham, S.G., 1987. Calibration of unsaturation patterns in long-chain ketone compositions for paleotemperature assessment. Nature 330, 367–369.

Pujos-Lamy, A., 1977. Essai d'établissement d'une biostratigraphie du nannoplancton calcaire dans le Pleistocéne de l'Atlantique Nord-oriental. Boreas 6, 323–331.

Qin, W., Carlson, L.T., Armbrust, E.V., Devol, A.H., Moffett, J.W., Stahl, D.A., Ingalls, A.E., 2015. Confounding effects of oxygen and temperature on the TEX$_{86}$ signature of marine Thaumarchaeota. Proceedings of the National Academy of Sciences of the United States of America 112, 10979–10984.

Raffi, I., Backman, J., Fornaciari, E., Palike, H., Rio, D., Lourens, L.J., Hilgen, F., 2006. A review of calcareous nannofossil astrobiochronology encompassing the past 25 million years. Quaternary Science Reviews 25, 3113–3137.

Rampen, S.W., Schouten, S., Wakeham, S.G., Sinninghe Damsté, J.S., 2007. Seasonal and spatial variation in the sources and fluxes of long chain diols and mid-chain hydroxy methyl alkanoates in the Arabian Sea. Organic Geochemistry 38, 165–179.

Rampen, S.W., Schouten, S., Sinninghe Damsté, J.S., 2011. Occurrence of long chain 1,14-diols in *Apedinella radians*. Organic Geochemistry 42, 572–574.

Rampen, S.W., Willmott, V., Kim, J.-H., Uliana, E., Mollenhauer, G., Schefuss, E., Sinninghe Damsté, J.S., Schouten, S., 2012. Long chain 1,13- and 1,15-diols as a potential proxy for palaeotemperature reconstruction. Geochimica et Cosmochimica Acta 84, 204–216.

Rampen, S.W., Willmott, V., Kim, J.-H., Rodrigo-Gámiz, M., Uliana, E., Mollenhauer, G., Schefuss, E., Sinninghe Damsté, J.S., Schouten, S., 2014a. Evaluation of long chain 1,14-alkyl diols in marine sediments as indicators for upwelling and temperature. Organic Geochemistry 76, 39–47.

Rampen, S.W., Datema, M., Rodrigo-Gámiz, M., Schouten, S., Reichart, G.-J., Sinninghe Damsté, J.S., 2014b. Sources and proxy potential of long chain alkyl diols in lacustrine environments. Geochimica et Cosmochimica Acta 144, 59–71.

Robinson, S.A., Ruhl, M., Astley, D.L., Naafs, B.D.A., Farnsworth, A.J., Bown, P.R., Jenkyns, H.C., Lunt, D.J., O'Brien, C., Pancost, R.D., Markwick, P.J., 2017. Early Jurassic North Atlantic sea-surface temperatures from TEX$_{86}$ palaeothermometry. Sedimentology 64, 215–230.

Rodrigo-Gámiz, M., Rampen, S.W., de Haas, H., Baas, M., Schouten, S., Sinninghe Damsté, J.S., 2015. Constraints on the applicability of the organic temperature proxies $U_{37}^{K'}$, TEX86 and LDI in the subpolar region around Iceland. Biogeosciences 12, 6573–6590.

Schouten, S., Hopmans, E.C., Schefuss, E., Sinninghe Damsté, J.S., 2002. Distributional variations in marine crenarchaeotal membrane lipids: a new tool for reconstructing ancient sea water temperatures? Earth and Planetary Science Letters 204, 265–274.

Schouten, S., Hopmans, E.C., Forster, A., van Breugel, Y., Kuypers, M.M.M., Sinninghe Damsté, J.S., 2003. Extremely high sea-surface temperatures at low latitudes during the middle Cretaceous as revealed by archaeal membrane lipids. Geology 31, 1069–1072.

Schouten, S., Hopmans, E.C., Sinninghe Damsté, J.S., 2004. The effect of maturity and depositional redox conditions on archaeal tetraether lipid palaeothermometry. Organic Geochemistry 35, 567–571.

Schouten, S., Huguet, C., Hopmans, E.C., Kienhuis, M.V.M., Sinninghe Damsté, J.S., 2007. Analytical methodology for TEX$_{86}$ paleothermometry by high-performance liquid chromatography/atmospheric pressure chemical ionization-mass spectrometry. Analytical Chemistry 79, 2940–2944.

Schouten, S., Baas, M., Hopmans, E.C., Reysenbach, A.-L., Sinninghe Damsté, J.S., 2008a. Tetraether membrane lipids of *Candidatus "Aciduliprofundum boonei"*, a cultivated obligate thermoacidophilic euryarchaeote from deep-sea hydrothermal vents. Extremophiles 12, 119–124.

Schouten, S., Baas, M., Hopmans, E.C., Sinninghe Damsté, J.S., 2008b. An unusual isoprenoid tetraether lipid in marine and lacustrine sediments. Organic Geochemistry 39, 1033–1038.

Schouten, S., Hopmans, E.C., Sinninghe Damsté, J.S., 2013. The organic geochemistry of glycerol dialkyl glycerol tetraether lipids: a review. Organic Geochemistry 54, 19–61.

Shimokawara, M., Nishimura, M., Matsuda, T., Akiyama, N., Kawai, T., 2010. Bound forms, compositional features, major sources and diagenesis of long chain, alkyl mid-chain diols in Lake Baikal sediments over the past 28,000 years. Organic Geochemistry 41, 753–766.

Sinninghe Damsté, J.S., Rijpstra, W.I.C., Hopmans, E.C., Prahl, F.G., Wakeham, S.G., Schouten, S., 2002. Distribution of membrane lipids of planktonic Crenarchaeota in the Arabian Sea. Applied and Environmental Microbiology 68, 2997–3002.

Sinninghe Damsté, J.S., Rampen, S.W., Rijpstra, W.I.C., Abbas, B., Muyzer, G., Schouten, S., 2003. A diatomaceous origin for long-chain diols and mid-chain hydroxy methyl alkanoates widely occurring in Quaternary marine sediments: indicators for high-nutrient conditions. Geochimica et Cosmochimica Acta 67, 1339–1348.

Sinninghe Damsté, J.S., Rijpstra, W.I.C., Hopmans, E.C., Jung, M.-Y., Kim, J.-G., Rhee, S.-K., Stieglmeier, M., Schleper, C., 2012. Intact polar and core glycerol dibiphytanyl glycerol tetraether lipids of Group I.1a and I.1b Thaumarchaeota in soil. Applied and Environmental Microbiology 78, 6866–6874.

Sinninghe Damsté, J.S., 2016. Spatial heterogeneity of sources of branched tetraethers in shelf systems: the geochemistry of tetraethers in the Berau River delta (Kalimantan, Indonesia). Geochimica et Cosmochimica Acta 186, 13–31.

Smith, M., de Deckker, P., Rogers, J., Brocks, J., Hope, J., Schmidt, S., Lopes dos Santos, R., Schouten, S., 2013. Comparison of $U_{37}^{K'}$, TEX$_{86}^{H}$ and LDI temperature proxies for reconstruction of south-east Australian ocean temperatures. Organic Geochemistry 64, 94–104.

Sorhannus, U., 2007. A nuclear-encoded small-subunit ribosomal RNA timescale for diatom evolution. Marine Micropaleontology 65, 1–12.

Spang, A., Hatzenpichler, R., Brochier-Armanet, C., Rattei, T., Tischler, P., Spieck, E., Streit, W., Stahl, D.A., Wagner, M., Schleper, C., 2010. Distinct gene set in two different lineages of ammonia-oxidizing archaea supports the phylum Thaumarchaeota. Trends in Microbiology 18, 331–340.

Sugai, A., Uda, I., Itoh, Y.H., Itoh, T., 2004. The core lipid composition of the 17 strains of hyperthermophilic archaea, *Thermococcales*. Journal of Oleo Science 53, 41–44.

Taylor, K.W.R., Huber, M., Hollis, C.J., Hernandez-Sanchez, M.T., Pancost, R.D., 2013. Re-evaluating modern and Palaeogene GDGT distributions: implications for SST reconstructions. Global and Planetary Change 108, 158–174.

ten Haven, H.L., Baas, M., de Leeuw, J.W., Schenck, P.A., Brinkhuis, H., 1987. Late Quaternary Mediterranean sapropels II. Organic geochemistry and palynology of S1 sapropels and associated sapropels. Chemical Geology 64, 149–167.

ten Haven, H.L., Rullkötter, J., 1991. Preliminary lipid analysis of sediments recovered during Leg 117. In: Prell, W.L., Niitsuma, N., Meyers, P.A., Emeis, K.C. (Eds.), Proceedings of the Ocean Drilling Program, Scientific Results, vol. 117. Ocean Drilling Program, College Station, Texas, pp. 561–569.

ten Haven, H.L., Eglinton, G., Farrimond, P., Kohnen, M.E.L., Poynter, J.G., Rullkötter, J., Welte, D.H., 1992. Variations in the content and composition of organic matter in sediments underlying active upwelling regimes: a study from ODP Legs 108, 112, and 117. Geological Society, London, Special Publications 64, 229–246.

Thierstein, H.R., Geitzenauer, K.R., Molfino, B., 1977. Global synchroneity of Late Quaternary coccolith datum levels – validation by oxygen isotopes. Geology 5, 400–404.

Tierney, J.E., Tingley, M.P., 2014. A Bayesian, spatially-varying calibration model for the TEX$_{86}$ proxy. Geochimica et Cosmochimica Acta 127, 83–106.

Versteegh, G.J.M., Bosch, H.-J., de Leeuw, J.W., 1997. Potential palaeoenvironmental information of C_{24} to C_{36} mid-chain diols, keto-ols and mid-chain hydroxy fatty acids: a critical review. Organic Geochemistry 27, 1–13.

Versteegh, G.J.M., Jansen, J.H.F., de Leeuw, J.W., Schneider, R.R., 2000. Mid-chain diols and keto-ols in SE Atlantic sediments: a new tool for tracing past sea surface water masses? Geochimica et Cosmochimica Acta 64, 1879–1892.

Volkman, J.K., Eglinton, G., Corner, E.D.S., Sargent, J.R., 1980. Novel unsaturated straight-chain C_{37}–C_{39} methyl and ethyl ketones in marine sediments and a coccolithophore *Emiliania huxleyi*. Physics and Chemistry of the Earth 12, 219–227.

Volkman, J.K., Barrett, S.M., Dunstan, G.A., Jeffrey, S.W., 1992. C_{30}–C_{32} alkyl diols and unsaturated alcohols in microalgae of the class Eustigmatophyceae. Organic Geochemistry 18, 131–138.

Volkman, J.K., Barrett, S.M., Blackburn, S.I., Sikes, E.L., 1995. Alkenones in *Gephyrocapsa oceanica* – implications for studies of paleoclimate. Geochimica et Cosmochimica Acta 59, 513–520.

Volkman, J.K., Barrett, S.M., Blackburn, S.I., 1999. Eustigmatophyte microalgae are potential sources of C_{29} sterols, C_{22}–C_{28} *n*-alcohols and C_{28}–C_{32} *n*-alkyl diols in freshwater environments. Organic Geochemistry 30, 307–318.

Warnock, J.P., Bauersachs, T., Kotthoff, U., Brandt, H.-T., Andren, E., 2017. Holocene environmental history of the Angermanalven Estuary, northern Baltic Sea. Boreas 47, 593–608.

Weijers, J.W.H., Schouten, S., Spaargaren, O.C., Sinninghe Damsté, J.S., 2006. Occurrence and distribution of tetraether membrane lipids in soils: implications for the use of the TEX_{86} proxy and the BIT index. Organic Geochemistry 37, 1680–1693.

Weijers, J.W.H., Schouten, S., van den Donker, J.C., Hopmans, E.C., Sinninghe Damsté, J.S., 2007. Environmental controls on bacterial tetraether membrane lipid distribution in soils. Geochimica et Cosmochimica Acta 71, 703–713.

Weller, P., Stein, R., 2008. Paleogene biomarker records from the central Arctic Ocean (Integrated Ocean Drilling Program Expedition 302): organic carbon sources, anoxia, and sea surface temperature. Paleoceanography 23, PA1S17. https://doi.org/10.1029/2007PA001472.

Willmott, V., Rampen, S.W., Domack, E., Canals, M., Sinninghe Damsté, J.S., Schouten, S., 2010. Holocene changes in *Proboscia* diatom productivity in shelf waters of the north-western Antarctic Peninsula. Antarctic Science 22, 3–10.

Wuchter, C., Schouten, S., Coolen, M.J.L., Sinninghe Damsté, J.S., 2004. Temperature-dependent variation in the distribution of tetraether membrane lipids of marine Crenarchaeota: implications for TEX86 paleothermometry. Paleoceanography 19, PA4028. https://doi.org/10.1029/2004PA001041.

Xie, S.T., Liu, X.L., Schubotz, F., Wakeham, S.G., Hinrichs, K.-U., 2014. Distribution of glycerol ether lipids in the oxygen minimum zone of the Eastern Tropical North Pacific Ocean. Organic Geochemistry 71, 60–71.

Yamamoto, M., Ficken, K., Baas, M., Bosch, H.-J., de Leeuw, J.W., 1996. Molecular palaeontology of the earliest Danian at Geulhemmerberg (the Netherlands). Geologie En Mijnbouw 75, 255–267.

Yang, H., Pancost, R.D., Tang, C.Y., Ding, W.H., Dang, X.Y., Xie, S.C., 2014. Distributions of isoprenoid and branched glycerol dialkanol diethers in Chinese surface soils and a loess-paleosol sequence: implications for the degradation of tetraether lipids. Organic Geochemistry 66, 70–79.

Zachos, J.C., Dickens, G.R., Zeebe, R.E., 2008. An early Cenozoic perspective on greenhouse warming and carbon-cycle dynamics. Nature 451, 279–283.

Zell, C., Kim, J.-H., Balsinha, M., Dorhout, D., Fernandes, C., Baas, M., Sinninghe Damsté, J.S., 2014. Transport of branched tetraether lipids from the Tagus River basin to the coastal ocean of the Portuguese margin: consequences for the interpretation of the MBT/CBT paleothermometer. Biogeosciences 11, 5637–5655.

Zhang, Y.G., Zhang, C.L., Liu, X.-L., Li, L., Hinrichs, K.-U., Noakes, J.E., 2011. Methane Index: A tetraether archaeal lipid biomarker indicator for detecting the instability of marine gas hydrates. Earth and Planetary Science Letters 307, 25–534.

Zhu, C., Weijers, J.W.H., Wagner, T., Pan, J.-M., Chen, J.-F., Pancost, R.D., 2011. Sources and distributions of tetraether lipids in surface sediments across a large river-dominated continental margin. Organic Geochemistry 42, 376–386.

Zhu, C., Meador, T.B., Dummann, W., Hinrichs, K.-U., 2014. Identification of unusual butanetriol dialkyl glycerol tetraether and pentanetriol dialkyl glycerol tetraether lipids in marine sediments. Rapid Communications in Mass Spectrometry 28, 332–338.

Zhu, C., Wakeham, S.G., Elling, F.J., Basse, A., Mollenhauer, G., Versteegh, G.J.M., Könneke, M., Hinrichs, K.-U., 2016. Stratification of archaeal membrane lipids in the ocean and implications for adaptation and chemotaxonomy of planktonic archaea. Environmental Microbiology 18, 4324–4336.